EARTH SURFACE PROCESSES AND LANDFORMS
Earth Surf. Process. Landforms **39**, 38–61 (2014)

Published online 11 November 2013 in Wiley Online Library
(wileyonlinelibrary.com) DOI: 10.1002/esp.3462

State of Science

The stream power river incision model: evidence, theory and beyond

Dimitri Lague*
Géosciences Rennes, Université Rennes 1, CNRS UMR 6118, Rennes Cedex, France

Received 13 February 2013; Revised 12 June 2013; Accepted 1 July 2013

*Correspondence to: Dimitri Lague, Géosciences Rennes, Université Rennes 1, UMR6118 CNRS, Campus de Beaulieu, 35042 Rennes Cedex, France.
E-mail: Dimitri.Lague@univ-rennes1.fr

ESPL
Earth Surface Processes and Landforms

ABSTRACT: The stream power incision model (SPIM) is a cornerstone of quantitative geomorphology. It states that river incision rate is the product of drainage area and channel slope raised to the power exponents m and n, respectively. It is widely used to predict patterns of deformation from channel long profile inversion or to model knickpoint migration and landscape evolution. Numerous studies have attempted to test its applicability with mixed results prompting the question of its validity. This paper synthesizes these results, highlights the SPIM deficiencies, and offers new insights into the role of incision thresholds and channel width. By reviewing quantitative data on incising rivers, I first propose six sets of field evidence that any long-term incision model should be able to predict. This analysis highlights several inconsistencies of the standard SPIM. Next, I discuss the methods used to construct physics-based long-term incision laws. I demonstrate that all published incising river datasets away from knickpoints or knickzones are in a regime dominated by threshold effects requiring an explicit upscaling of flood stochasticity neglected in the standard SPIM and other incision models. Using threshold-stochastic simulations with dynamic width, I document the existence of composite transient dynamics where knickpoint propagation locally obeys a linear SPIM (n=1) while other part of the river obey a non-linear SPIM (n>1). The threshold-stochastic SPIM resolves some inconsistencies of the standard SPIM and matches steady-state field evidence when width is not sensitive to incision rate. However it fails to predict the scaling of slope with incision rate for cases where width decreases with incision rate. Recent proposed models of dynamic width cannot resolve these deficiencies. An explicit upscaling of sediment flux and threshold-stochastic effects combined with dynamic width should take us beyond the SPIM which is shown here to have a narrow range of validity. Copyright © 2013 John Wiley & Sons, Ltd.

KEYWORDS: river incision; channel geometry; knickpoints; stochastic models

Introduction

Given the central role of rivers in shaping landscapes, understanding river evolution over geological timescales is one of the key goals of quantitative geomorphology. As such, mathematical river incision models are critical to establish a quantitative link between tectono-climatic perturbations and the temporal evolution of channel geometry and drainage networks. Several models of river incision have been proposed, but by far, the most commonly used approach is based on the stream power incision model (SPIM) in which the long-term river downcutting rate I is given by:

$$I = KA^m S^n, \tag{1}$$

in which K is often called erodibility and is a measure of incision efficiency, A is upstream drainage area, S is the topographic slope and m, n are exponents. To predict channel evolution, Equation 1 is generally coupled to a detachment-limited mass balance equation in which:

$$\frac{dh}{dt} = U - I = U - KA^m \left(\frac{dh}{dx}\right)^n, \tag{2}$$

where h is the elevation of the bedrock bed, t the time, x is the downstream distance and U is the rate of baselevel lowering (i.e. the rock uplift rate if the baselevel is at constant elevation) (Howard and Kerby, 1983; Howard, 1994; Whipple and Tucker, 1999).

Equations 1 and 2 are now part of the landscape of geomorphology and are routinely used in many applications. In particular, the SPIM is commonly used to map river incision rates and infer uplift patterns [assuming steady-state (SS), that is $U = I$] (e.g. Kirby and Whipple, 2012; Lavé and Avouac, 2001; Wobus *et al.*, 2006), interpret relationships between catchment denudation rates and channel geometry (DiBiase and Whipple, 2011; Safran *et al.*, 2005), model knickpoint migration (e.g. Berlin and Anderson,

2007; Crosby and Whipple, 2006), reconstruct paleotopography (e.g. Harkins *et al.*, 2007; Sternai *et al.*, 2012) and past-changes in baselevel rate (e.g. Roberts and White, 2010), or model topographic evolution at catchment and orogen scale (e.g. Garcia-Castellanos and Villaseñor, 2011; Herman and Braun, 2006; Roe *et al.*, 2003; Whipple and Meade, 2006). The strength of the SPIM is to reproduce many elements of SS and transient river profiles with a simple model formulation. For instance, the downstream decrease of channel slope with drainage area often observed in nature is well reproduced if $m/n \sim 0.5$ and $U = I$. Equations 1 and 2 can produce upstream propagating knickpoints observed in nature. The SPIM is also based on simple geometrical parameters (channel slope and drainage area) that can be estimated from digital elevation models (DEM). Moreover, the SPIM can be derived from a reasonable set of assumptions regarding channel hydraulics, catchment hydrology, and incision processes depending on shear stress (Whipple and Tucker, 1999; Whipple *et al.*, 2000) or from simple energetic considerations (i.e., as the unit rate of energy expenditure on the channel bed and banks yielding $m = 0.5$ and $n = 1$). This combination of theory, simplicity, and consistency with observations explain the exceptional endorsement of the SPIM by the geomorphology community and beyond (as of 2013, about 40–50 papers per year cite Howard, 1994 and Whipple and Tucker, 1999).

Yet, it has been known since the infancy of the model that the SPIM described in Equations 1 and 2 is likely to be too simple to be universal. Many field and experimental examples point towards its inability to capture important aspects of channel dynamics such as channel width variation with incision rates (e.g. Lavé and Avouac, 2001; Whittaker *et al.*, 2007b) or the impact of sediment supply in driving or inhibiting incision (e.g. Cook *et al.*, 2013; Finnegan *et al.*, 2007; Sklar and Dietrich, 2001; Turowski *et al.*, 2008b). Theoretical studies have also pointed out weaknesses in the original derivation of the model and its treatment of erosion threshold in the context of stochastic discharge (e.g. Lague *et al.*, 2005; Snyder *et al.*, 2003b; Tucker, 2004). Despite these contradictory elements, the simple linear SPIM (with $n = 1$) remains widely used. It thus becomes important to confront it to a decade of new quantitative constraints and theoretical developments. This is the main objective of this work organized in three parts. I first synthesize a broad range of quantitative field constraints into six sets of empirical evidence that any incision model (SPIM or other) should be able to reproduce to reach a minimal level of universality. These include SS and transient properties of incising channels. The second part addresses the theoretical basis of the SPIM through a discussion of the derivation of long-term geomorphic laws from physics principles. A re-analysis of published field data highlights the dominant role of threshold effects combined with stochastic floods and numerical simulations illustrate a previously unforeseen complexity introduced by these effects during transient dynamics. The third part confronts the theoretical predictions with the six groups of field evidence. I conclude by identifying a series of critical issues that should be addressed to improve the modelling of long-term river incision.

For the sake of conciseness, I assume that the reader is already aware of SPIM applications and of the existence of other incision models such as the transport-limited model. If not, I suggest to first read a series of recent reviews of topics connected to the SPIM: bedrock rivers (Turowski, 2012; Whipple *et al.*, 2013), landscape evolution modelling (Tucker and Hancock, 2010) and tectonic geomorphology (Burbank and Anderson, 2012; Kirby and Whipple, 2012).

Field Constraints and an Empirical SPIM

By reviewing a list of field examples on the SS geometry and transient dynamics of incising rivers, I follow two objectives: (1) to identify a minimum set of six field constraints that any universal long-term incision model, including the SPIM, should at least be able to predict; and (2) to evaluate how a purely empirical SPIM constructed from Equations 1 and 2 can account for these constraints independently from any underlying physics principle.

Ideally, one should compare the scaling of channel geometry directly with discharge characteristics (mean annual discharge and variability) rather than drainage area (this will be justified in the next section). However given the limited number of points where discharge is precisely recorded in mountain areas, this is generally not feasible. Precipitation patterns are also crudely known in mountainous area, even if satellite data can now bring more constraints (e.g. Bookhagen and Burbank, 2006). But the prediction of discharge from spatio-temporal rainfall variations is a complex problem that has no simple solution yet [see discussion by Tucker and Hancock (2010) in the context of landscape evolution modelling]. It is also even questionable to relate decadal hydrological conditions to the present day river geometry resulting from the integrated effect of thousands of years of incision events under potentially different climate conditions. For this reason and because Equation 1 is generally expressed in term of drainage area, I choose to use the raw data generally published: slope, width and drainage area.

Evidence 1: scaling of channel slope with drainage area at steady-state

Rivers (or segment of rivers) incising through uniformly uplifting rocks, under approximately uniform precipitation rates and lithology and which are likely close to a SS configuration are characterized by:

$$S = k_s A^{-\theta}, \tag{3}$$

which is known as Flint's law (Flint, 1974), where k_s is the channel steepness index (Snyder *et al.*, 2000), and θ is the concavity index. No systematic compilation of θ exists allowing to pinpoint what is the mostly likely value of θ (independently of any a priori theoretical expectations), but a range of 0.4 to 0.6 is often reported (e.g. Kirby and Whipple, 2012; Whipple, 2004). Detailed studies in which uplift was the only factor varying between catchments in the same area have demonstrated that θ does not vary with uplift rate or lithology in a statistically significant way (e.g. Duvall *et al.*, 2004; Kirby and Whipple, 2001; Lague *et al.*, 2000; Ramsey *et al.*, 2006; Snyder *et al.*, 2000). Moreover, given the different climate regimes in which Equation 3 has been reported, and the narrow range in which θ falls, one can consider that an outcome of any incision model is that Equation 3 must be verified with θ of the order of 0.5 at SS.

Note that Equation 3 only applies above a critical drainage area of the order of 0.1 to 5 km^2 below which colluvial processes (debris flows, landsliding) dominate fluvial processes (e.g. Lague and Davy, 2003; Montgomery and Foufoula-Georgiou, 1993; Ramsey *et al.*, 2006; Snyder *et al.*, 2003a; Stock and Dietrich, 2003). Similarly, in cases where the river changes from incision to deposition, parameters of Flint's law are expected to be different. Finally, the inherent noise in DEMs can strongly affect the estimate of θ and k_s and proper processing methods as well as error estimation should systematically be performed (e.g. Wobus *et al.*, 2006a).

Demonstrating that a given river or reach is at SS remains difficult. It has been directly documented in a few cases by showing that rates of river incision or catchment denudation are about steady over several thousand of years (Cyr and Granger, 2008; Lavé and Avouac, 2001). The tendency for incising rivers to reach SS is also expected from the slope sensitivity of incision rate (see next sub-section). Even complex stochastic river incision models with explicit bed and bank incision, reduction of incision by sediment transport, and driven by daily fluctuations of sediment and water discharge reach an average SS geometry where vertical incision rate averaged over hundreds of years matches a constant imposed uplift rate (e.g. Lague, 2010). However, our ability to assess SS in nature from simple geometrical constraints relies on inferences drawn from numerical simulations and presuppose an underlying incision model. Hence, one often refers to a combination of three elements: the absence of knickpoints, a smooth concave-up profile with θ close to 0.5 and the knowledge that uplift have been constant for a long-time (e.g. Duvall *et al.*, 2004; Snyder *et al.*, 2000; Whittaker *et al.*, 2007b) or that is has changed extremely slowly and that a quasi-SS assumption applies (e.g. Whipple and Meade, 2006). Yet, the first two assumptions already presuppose that the SPIM model applies. Hence, while the presence of knickpoints or off-the-charts concavity index is a signature of the violation of one key assumption (spatial uniformity of boundary conditions or SS), their absence is not proof of SS.

It can be shown easily that a SPIM model (Equation 2) predicts $\theta = m/n$ as long as the incision rate is spatially uniform (e.g. Snyder *et al.*, 2000; Whipple and Tucker, 1999). Any combination of n and m verifying $n \sim 2m$ thus yield a valid SPIM.

Evidence 2: sensitivity of slope to incision rate at steady-state

The sensitivity of channel slope to incision rate is best assessed using the channel steepness index k_s which accounts for drainage area sensitivity. Care must be taken to reduce noise effects from DEMs by calculating slope along the river profile (as opposed to by the steepest descent) and averaging the channel profile over a large enough distance (e.g. Wobus *et al.*, 2006a). Alternatively, a recent technique called the 'integral approach' has been developed to avoid the computation of slope on noisy elevation data (Harkins *et al.*, 2007; Perron and Royden, 2013). It is based on the renormalization of the river long profile. To date, the integral approach has not yielded results that are fundamentally different from those obtained through a slope-area analysis.

A reference concavity exponent of $\theta = 0.45$ is now routinely used to compare channel profiles and individual reaches from different locations (Whipple, 2004; Whipple *et al.*, 2013; Wobus *et al.*, 2006a). In that case k_s=k_{sn} and is called the normalized steepness. Figure 1 presents a compilation of various studies illustrating the range of k_{sn} found on earth and its sensitivity to incision rate (see Appendix A for a discussion on the nature and quality of the incision rate constraints). This compilation is restricted to three types of studies: strath terrace derived incision rates for which the local slope and drainage area of the river is known (Lavé and Avouac, 2001; Yanites *et al.*, 2010b); uplift derived incision rates studies for which k_{sn} for $\theta = 0.45$ was given or could be backcalculated (Duvall *et al.*, 2004; Kirby and Whipple, 2001, 2012; Snyder *et al.*, 2000); studies using denudation rates derived from detrital cosmogenics radionuclide (CRN) in which the authors have checked that rivers did not exhibit features such as knickpoint

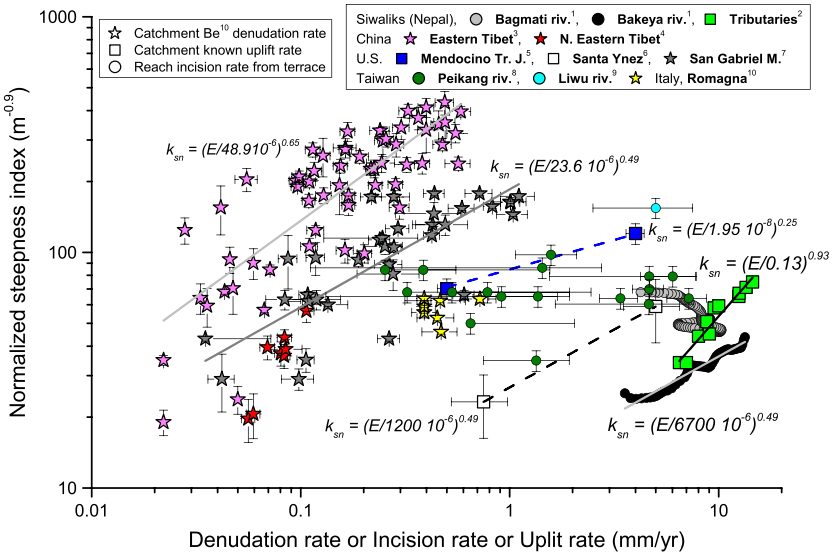

Figure 1. Compilation of published data of normalized channel steepness index k_{sn} versus river incision rate, catchment denudation rate or uplift rate. If, as argued in these various studies, the landscape is close or at steady-state, these different rates should all measure the rate of channel incision. Two different sources of data are also presented: steepness derived from the regression over the complete channel profile (for denudation rates and catchment known uplift rate) and local estimate of steepness for reaches in which the incision rate is known (reach incision rate from terrace). Note that the Bagmati River and Peikang River data do not exhibit a significant variation of k_{sn} with incision rate. Only the Siwaliks tributaries exhibit a nearly linear relationship, while the other dataset (provided that they cover a range of incision rates large enough) exhibit a less than linear dependency (quite often $k_{sn} \sim I^{0.5}$). Data sources: **1**, digitized from (Lavé and Avouac, 2001) using a constant drainage area A = 3200 km^2, for the Bagmati, and A = 320 km^2 for the Bakeya (plot uses one point every 250 m); **2**, (Kirby and Whipple, 2001 re-analysed in Wobus *et al.*, 2006a); **3**, digitized from (Ouimet *et al.*, 2009); **4**, digitized from (Harkins *et al.*, 2007); **5**, (Snyder *et al.*, 2000); **6**, (Duvall *et al.*, 2004); **7**, (DiBiase *et al.*, 2010); **8**, (Yanites *et al.*, 2010b); **9**, incision rate is supposed to be equal to long-term exhumation rate and errors bars are set at 50% to reflect this large uncertainty (Hartshorn *et al.*, 2002); **10**, (Cyr *et al.*, 2010), only the dataset from Romagna is used to compare data on the same lithology. Power-law regression were obtained from linear fits on log-transformed data and are given as a general indication of the non-linearity degree given that most dataset are relatively noisy. This figure is available in colour online at wileyonlinelibrary.com/journal/espl

or convex reaches and for which there is a limited variation in precipitation and rock lithology [this excludes studies such as Bookhagen and Strecker (2012); Safran *et al.* (2005), and I choose only one lithology for the data from Cyr *et al.* (2010)]. While the source of data varies widely, if SS conditions prevails as argued in these studies, then all these measures should be comparable. Note also that some data points correspond to a steepness value obtained for a supposedly uniform catchment, while others corresponds to individual channel reaches along rivers crossing gradients in uplift rates. The position of a channel reach of the Liwu River in Taiwan is also indicated as it has been used in many studies pertaining to bedrock incision processes (Hartshorn *et al.*, 2002; Lague, 2010; Turowski *et al.*, 2008b; Wilson *et al.*, 2013). Figure 1 illustrates several important aspects both in terms of the range of steepness currently met in orogenic areas and on the inference that can be made on the sensitivity of channel slope to incision rate.

First, the two large CRN datasets (DiBiase *et al.*, 2010; Ouimet *et al.*, 2009) exhibit a monotonic increase of steepness with denudation rate but more importantly a significant variability for a given denudation rate especially at sub 0.1 mm/yr rates. This variability may reflect natural heterogeneity in boundary conditions despite careful choice of the catchments or intrinsic variability of the CRN method (due to stochastic landsliding, imperfect SS conditions, e.g. Niemi *et al.*, 2005; Yanites *et al.*, 2009). Yet, it underlines that only datasets covering a large range of denudation rates are likely to yield relevant information if any correlation is expected to emerge. As such, small datasets should arguably only be used to place a constraint on the range of denudation rates corresponding to a given steepness (e.g. Cyr *et al.*, 2010; Harkins *et al.*, 2007). Figure 1 also highlights the current hiatus in the range of rates that different techniques can cover: CRN derived denudation rates are restricted to sub mm/yr values while other source of well-documented data tend to be for incision rates or uplift rates greater than 1 mm/yr. While there seems to be an apparent gap in the 100 to 500 $m^{-0.9}$ range of k_{sn} for incision rates greater than 1 mm/yr, we note that Central and High Himalayan rivers developed on more resistant rocks than the Siwaliks hills likely fall in this region given the range of documented exhumation rates (Wobus *et al.*, 2003).

Figure 1 shows that all but two datasets (Bagmati River crossing the Siwaliks Hills and Peikang River, Taiwan) report a monotonic increase of channel steepness with incision rate (Cyr *et al.*, 2010; DiBiase *et al.*, 2010; Kirby and Whipple, 2001; Lague *et al.*, 2000; Safran *et al.*, 2005; Snyder *et al.*, 2000). In part driven by theoretical considerations (see next section) and more recently by observational evidence (e.g. DiBiase and Whipple, 2011; Kirby and Whipple, 2012; Ouimet *et al.*, 2009), a power-law model is often used to model the data when a correlation exists:

$$k_{sn} = \left[\frac{I}{I_{sref}}\right]^{\varphi}, \tag{4}$$

where φ is the steepness-incision scaling exponent, and I_{sref} is a reference incision rate measuring incision efficiency. φ is apparently not unique and ranges from 0.25 (Snyder *et al.*, 2003b, without correction for orographic precipitation), over ~ 0.5 (DiBiase *et al.*, 2010; Duvall *et al.*, 2004; Lavé and Avouac, 2001; Ouimet *et al.*, 2009; Snyder *et al.*, 2003b with orographic correction) to ~ 1 (Wobus *et al.*, 2006a). Safran *et al.* (2005) reports a poorly defined linear dependency between steepness index and denudation rate, that can be equally well fit by a non-linear relationship with φ ~ 0.5, and as such provides little constraints on scaling. Hence, only the Siwaliks tributaries exhibit a nearly linear relationship over a two-fold change in uplift rate. Quite importantly, the Bagmati River in the Siwaliks Hills of Nepal (Lavé and Avouac, 2001) and the Peikang River dataset in Taiwan (Yanites *et al.*, 2010b) exhibit no clear trend between k_{sn} and the rate of incision (or even a slight inverse correlation for the Bagmati at the entrance of the gorge) yielding φ ~ 0. These two datasets correspond to rivers developed over non-uniform uplift, which are currently covered by a significant thickness of sediment (2 to 15 m for the Peikang River, Yanites *et al.*, 2011). Even though the SS assumption is not fully validated for the Peikang River, Figure 1 shows that it does not have a particularly low or high steepness. The Bakeya River which is also crossing non-uniform uplift exhibits φ ~ 0.5, even though it is also largely covered by sediment at present (Lavé and Avouac, 2001).

This data compilation highlights an important result: channel steepness only increases linearly with incision rate in one dataset. Indeed the fact that most datasets predict φ significantly smaller than one is consistent with the range of k_{sn} reported on earth covering a little more than one-order of magnitude (from ~ 20 to 500 $m^{-0.9}$) for nearly three orders of magnitude change in incision rates (0.02 to 14 mm/yr) (Figure 1 and Whipple, 2004). This underlines that channel steepness cannot increase linearly with incision rate for all ranges of incision rates, even if a fraction of rivers in the world with different rocks, climate regimes and sediment fluxes are sampled in Figure 1.

It can be shown easily that a SPIM predicts $\varphi = 1/n$ (Snyder *et al.*, 2000). The previous analysis thus shows that an empirical calibration of n from SS data would predict $n \sim 2$ (and thus $m \sim 1$) for most cases but three: the Siwaliks tributaries ($n = 1$) and the Bagmati and Peikang Rivers. In these two latter cases the lack of slope variation with incision rate has long been recognized as a major failure of the SPIM (Lavé and Avouac, 2001). Indeed, for the Bagmati and Peikang Rivers, alongstream changes in rates of incision are accommodated geometrically by changes in channel width. This justifies the inclusion of the scaling of channel width with drainage area and incision rate as additional evidence that any universal incision model should account for. In the absence of an explicit description of channel width in Equations 1 and 2, the empirical SPIM exponents are fully calibrated with the slope information, and yield for most cases $m \sim 1$ and $n \sim 2$, with one evidence for $m \sim 0.55$ and $n \sim 1.1$ (Siwaliks Tributaries), $m \sim 0.85$ and $n \sim 1.7$ (Eastern Tibet data) and $m \sim 2$ and $n \sim 4$ (Mendocino Triple Junction).

Evidence 3: scaling of channel width at steady-state

In a catchment with uniform precipitation, lithology, and incision rate, the width of incising channels scales with drainage area as:

$$W = k_w A^b, \tag{5}$$

where k_w can be thought (in comparison to the steepness index) as a width index (Turowski *et al.*, 2006; Yanites and Tucker, 2010) and b the width-area scaling exponent (e.g. Duvall *et al.*, 2004; Montgomery and Gran, 2001; Snyder *et al.*, 2003b). Given that many channels have banks which are not vertical, one difficulty in estimating the parameters of Equation 5 is to be sure that the width is measured for a comparable discharge between sites. Compared to alluvial rivers for which alluvial banks serve as a natural reference flow depth, there is no such markers in bedrock walled rivers apart from scour marks and limits of vegetation. Given that scour marks

can be largely set by the last flood event (Turowski *et al.*, 2008b), one should be cautious when comparing channel width between sites, especially for narrow rivers. Recent reviews and papers (Comiti *et al.*, 2009; DiBiase and Whipple, 2011; Turowski *et al.*, 2009; Whipple *et al.*, 2013; Whittaker *et al.*, 2007a; Yanites and Tucker, 2010) report values of b between 0.25 and 0.6 and a significant variability of channel width within a catchment at a given drainage area. To my knowledge only four studies have carefully studied channel width in the context of incising bedrock channels with uniform precipitation and lithology and likely SS conditions (DiBiase and Whipple, 2011; Duvall *et al.*, 2004; Snyder *et al.*, 2003a; Whittaker *et al.*, 2007a). They yield an average of $b = 0.35 \pm 0.11$ (representing seven different sites). These estimates concentrate on channels that are not larger than 10 m and small catchments (typically 1–100 km^2) for which drainage area likely scales linearly with mean annual discharge. As such b is indicative of the scaling with discharge which is lower than the typical scaling observed for alluvial channel $b = 0.5$ (using bankfull discharge rather than drainage area) (Knighton, 1998; Leopold and Maddock, 1953). Assessing b for larger catchments is complicated by the non-uniformity of lithology, uplift or precipitation. Yanites *et al.* (2010b) report $b = 0.54$ for the Peikang River in Taiwan. Pooling of several different sources over a larger range of drainage areas yield $b = 0.32$ (Wohl and David, 2008), although the concavity exponent for the same set of data is 0.26 questioning the relevance of averaging widely different settings. Hence, while narrow and steep bedrock rivers seem to have a different scaling behaviour with drainage area than alluvial rivers, it remains an open question for wide bedrock rivers (Montgomery and Gran, 2001; Wohl and David, 2008).

Another important SS property of river channels is how flow width varies at a given location with increasing discharge, known as the at-a-station hydraulic geometry (Leopold and Maddock, 1953). Starting to look at the at-a-station hydraulic geometry might seem a little far from reach scale model of long-term incision, but this relationship is one element controlling how the shear-stress exerted by the water flow on the river bed scales with discharge at a given location. The other component depends on the relative contribution of bank and bed friction on the total friction opposed to the flow. As discussed in the modelling section, these two elements are highly relevant to the correct theoretical derivation of long-term incision models (DiBiase and Whipple, 2011; Lague *et al.*, 2005; Tucker, 2004). The at-a-station hydraulic geometry is also one characteristic that is expected to be significantly distinct from alluvial rivers: because bedrock channels are generally confined within walls, bed shear stress is continuously increasing with discharge (except maybe in the limiting case of narrow gorges where bank friction might buffer bed shear stress during large flood events, e.g. Turowski *et al.*, 2008b). In an alluvial river, overbank flow limits the increase of flow velocity with discharge and therefore imposes a break in the scaling behaviour of bed shear stress with discharge.

An extensive study of gauging station records of bedrock rivers in Taiwan (Turowski *et al.*, 2008a) shows that their at-a-station hydraulic geometry is adequately described by a power-law:

$$\frac{W(Q)}{W} = \left(\frac{Q}{Q_{ref}}\right)^{\omega_s}, \tag{6}$$

where $W(Q)$ is flow width at discharge Q, Q_{ref} is the reference discharge at which W is measured, and ω_s is the at-a-station width scaling exponent which can be roughly thought as a measure of bank steepness (i.e. a rectangular channel would have $\omega_s = 0$). In 46 gauging stations located in incising bedrock rivers, ω_s varies between 0.15 to 0.55 with a mean value of 0.34. In Taiwan, ω_s is independent of drainage area, of the coefficient of variation of discharge but positively correlated with mean sediment concentration (Turowski *et al.*, 2008a). More field constraints on this important parameter are needed.

Evidence 4: scaling of channel width with incision rate at steady-state

Channel width appears to have different sensitivity to incision rate at steady state (Turowski *et al.*, 2009; Yanites and Tucker, 2010). This sensitivity, but also the relative width of channels in different settings, is best captured by considering a normalized width index similar to the normalized steepness index (Turowski *et al.*, 2006; Yanites and Tucker, 2010):

$$k_{wn} = \frac{W}{A^{b_{ref}}}, \tag{7}$$

where b_{ref} is a reference scaling exponent and where k_{wn} can be estimated locally, or from a fit through width-area data. Given the lack of consensus on the true scaling of width with discharge, I use b_{ref} =0.5 mainly because it makes k_{wn} adimensional. Figure 2 presents the values of k_{wn} for different published datasets (Turowski *et al.*, 2009; Yanites and Tucker, 2010). It highlights two different behaviours: cases in which channel width is insensitive to incision rate, as for the channel profiles developed over uniform boundary conditions of Snyder *et al.* (2003a) and DiBiase and Whipple (2011); and cases where channel width decreases with incision rate. This latter behaviour is systematic for river crossing non-uniform uplift zones but uniform lithology (Lavé and Avouac, 2001; Yanites *et al.*, 2010b) but is also observed for catchments developed over uniform uplift rates (Duvall *et al.*, 2004). In that latter case, spatial variations in coarse bedload supply may also amount as a change in boundary conditions (Whipple *et al.*, 2013). In at least two cases this narrowing can adequately be captured by a power-law relationship:

$$k_{wn} = \left[\frac{I}{I_{wref}}\right]^{-\chi} \tag{8}$$

where I_{wref} is a reference incision rate and χ the width-incision scaling exponent. In the Bakeya River, $\chi \sim 0.63$ (Turowski *et al.*, 2009) and $\chi \sim 0.4$ for the Peikang River (Yanites and Tucker, 2010). Additional empirical evidence is needed to further assess the expected functional relationship between width and incision rate (power-law or not) and the range of χ.

Transient dynamics of incising channels

Evidence 5: diversity of transient geometry

Perturbations taking the form of migrating knickpoints (KPs) have been documented in the context of rapid changes in relative baselevel fall rates and constitute an important evidence of channel dynamics that must be captured by an incision model. Relative baselevel can be defined locally by a confluence with a higher order stream, an active tectonic feature or regionally by sea level (Whipple *et al.*, 2013). These changes can be discrete (in which case the channel is expected to go back to

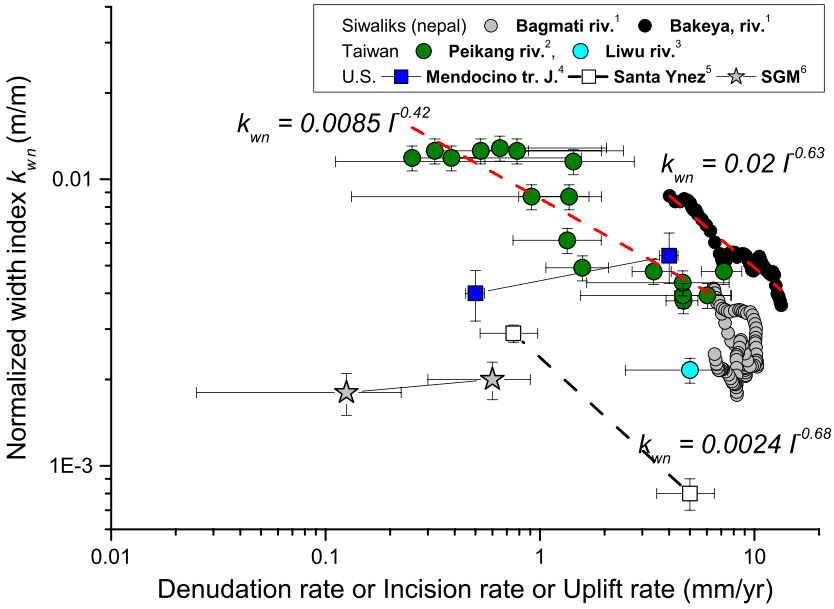

Figure 2. Normalized width index k_{wn} (channel width normalized by drainage area effects assuming $W \propto A^{0.5}$) versus denudation rate or incision rate or uplift rate (see Figure 1 and text for a discussion on the data source uncertainties). Two types of behaviour can be detected: catchment derived k_{wn} independent of uplift rate or denudation rate, and catchment derived or reach scale k_{wn} decreasing with incision rate. Channels crossing non-uniform uplift systematically narrow with incision rate. For identical drainage area, incising channels can have up to one-order of magnitude difference in channel width (e.g. Santa-Ynez Rivers and the Bakeya River). The Liwu River is indicated to show that it does not have any peculiar width or steepness index compared to other datasets. Data sources: **1**, digitized from (Lavé and Avouac, 2001); **2**, data from (Yanites *et al.*, 2010b, 2011) using Central Age Model incision rates; **3**, (Hartshorn *et al.*, 2002), a 30% uncertainty is attributed to the width measured for flood of annual recurrence; **4**; (Snyder *et al.*, 2003b) estimated from the reference high flow width at 1 km^2 (note that accounting for a two-fold change in precipitation rate between the high and low flow data makes the width index identical in both cases); **5**, digitized from (Duvall *et al.*, 2004); **6**, digitized from (DiBiase and Whipple, 2011). The large uncertainty in denudation rates reflect the fact that channel width data were classified between low steepness ($k_{sn} < 100$ with denudation rates $\in$ [0.035,0.3] mm/yr) and high steepness ($k_{sn} > 100$, with denudation rates $\in$ [0.3,1.1] mm/yr). This figure is available in colour online at wileyonlinelibrary.com/journal/espl

its initial SS condition or simply relax in the absence of permanent baselevel fall) or permanent (in which case a new SS is attained). KP propagation has been documented following local earthquake faulting (e.g. Cook *et al.*, 2013), increase in fault throw rate (e.g. Whittaker *et al.*, 2007b), changes in sea level or post-glacial rebound (e.g. Bishop *et al.*, 2005; Loget *et al.*, 2006) or in badlands (e.g. Howard and Kerby, 1983). Experiments provide several examples of the migration of KPs after instantaneous or permanent perturbations (e.g. Gardner, 1983; Lague *et al.*, 2003).

As argued by others (Burbank and Anderson, 2012; Haviv *et al.*, 2010; Kirby and Whipple, 2012), it is important to refine the KP notion in order to highlight the rich geometry of transient dynamics that incision model should match. Based on observations, transient channel geometries fall into three types (Figure 3): vertical step KP, slope-break KP and knickzones (Haviv *et al.*, 2010; Kirby and Whipple, 2012; Loget *et al.*, 2006; Whipple *et al.*, 2013). Vertical step KPs are very steep reaches (rapids) and waterfalls having a significantly higher slope than the average trend in a slope-area diagram or channel profile (Bishop *et al.*, 2005; Haviv *et al.*, 2010; Hayakawa and Matsukura, 2003; Korup, 2006; Seidl *et al.*, 1994). Slope-break KPs correspond to the local transition between upstream and downstream reaches with roughly identical concavity but different steepness indexes (Brocard and Van der Beek, 2006; Miller *et al.*, 2012; Wobus *et al.*, 2006a) or where at least the downstream part of the river exhibits a slope-area scaling with $\theta \sim 0.45$ (e.g. Berlin and Anderson, 2007). Knickzones correspond to downstream persistent change in channel concavity: straight to convex knickzones are frequently reported in which channel steepens downstream leading to very low or even negative concavity indexes (e.g. Harkins *et al.*, 2007; Loget *et al.*, 2006; Miller *et al.*, 2012; Ouimet *et al.*, 2007; Valla *et al.*, 2010). In this case, the term KP can be used to define the upstream termination of the knickzone (Loget and Van den Driessche, 2009; Whittaker and Boulton, 2012). Knickzones develop at least over several kilometres (Miller *et al.*, 2012; Valla *et al.*, 2010) to hundreds of kilometres (Loget *et al.*, 2006; Ouimet *et al.*, 2007), while KPs are local features (Figure 3).

Any of the previous anomalous geometries can be static and not characteristic of transient dynamics. Downstream variations in uplift rate or lithology can produce KPs or knickzones even at SS (Figure 3). For instance, the Bakeya River exhibits a convex knickzone over 6 km resulting from significant steepening in response to downstream increase in uplift rate (Lavé and Avouac, 2001). Vertical step and slope-break KP have been frequently identified at the transition between lithologies (e.g. Brocard and van der Beek, 2006).

The previous synthesis highlights a rich diversity of transient channel profile geometries representing a challenge for incision models to reproduce. The lack of systematic analysis of channel width in most published work tend to focus the problem of transience on KP development. However channel width represents an important but largely unexplored dimension of the problem, in particular when it comes to the problem of strath terrace formation (Hancock and Anderson, 2002): the frequent occurrence of paired strath terraces downstream of migrating KPs documents a concomitant narrowing and steepening of channel during transience. Similarly, all published data on convex knickzones systematically report over-narrowed reaches compared to normal hydrological scaling (i.e. k_{wn} decreasing) (Valla *et al.*, 2010; Whittaker and Boulton, 2012; Whittaker *et al.*, 2007a). These examples highlight the importance to document both profile and channel width variations in future studies.

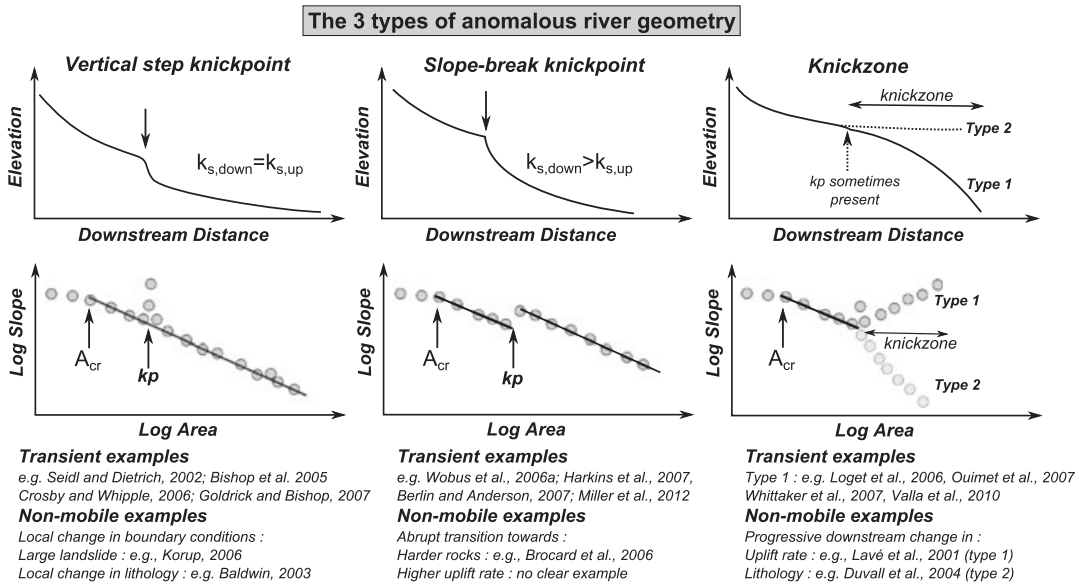

Figure 3. Classification of the three types of anomalous river geometry in long-profile and slope–area diagrams. These anomalies have been recognized in several studies as a transient (i.e. migrating upstream) or a non-mobile feature and should be reproduced by any incision model. The value of A_{cr} is the critical drainage area below which other processes dominate (e.g. debris-flow, landslides). Modified and expanded from (Burbank and Anderson, 2012; Haviv *et al.*, 2010; Whipple *et al.*, 2013; Wobus *et al.*, 2006a).

Evidence 6: controls on knickpoint migration rate

Drainage area has been identified as a dominant factor controlling the recession rate of vertical step KPs (Berlin and Anderson, 2007; Bishop *et al.*, 2005; Crosby and Whipple, 2006; Hayakawa and Matsukura, 2003; Jansen *et al.*, 2011), and KPs upstream of convex knickzones (Loget and Van den Driessche, 2009; Valla *et al.*, 2010) since their inception. In catchments with uniform lithology and precipitation, the retreat distance R scales generally very well with catchment drainage area (or tributary catchment area) as:

$$R = dA^{\varepsilon}, \tag{9}$$

where d and ε are parameters fitted to the data. Values for ε range from 0.34 in northeast Tibet (Harkins *et al.*, 2007), ~ 0.5 for Messinian Crisis KP (Loget and Van den Driessche, 2009), 0.69 in Scotland (Jansen *et al.*, 2011), 0.73 in Japan (Hayakawa and Matsukura, 2003),~ 0.8 for hanging valleys in the Alps (Valla *et al.*, 2010) to 1.26 in Scotland (Bishop *et al.*, 2005). Valla *et al.* (2010) by studying KP propagation on two types of rock lithology report a difference in d for identical exponents ε. Authors have also replicated the KPs position using a model of KP celerity $V$of the following form:

$$V = CA^{p}, \tag{10}$$

where C and p are parameters. KPs are propagated through a drainage network incrementally according to Equation 10 assuming a known timing and position of a baselevel fall. Crosby and Whipple (2006) found $p = 1.12$ for KPs developed into the mudstones of the Waipaoa Catchment (New Zealand). These authors also demonstrate that the present-day position of KPs can also be explained by a model in which channel incision efficiency decreases rapidly below a threshold drainage area. Berlin and Anderson (2007) found p ranging from 0.5 to 0.62. In both cases, a simple model such as Equation 10 performs extremely well. Note that if Equation 10 strictly applies during the transient evolution of a river, then $\varepsilon = p$.

Empirical SPIM derived from transient constraints

When $n = 1$, the detachment-limited SPIM (Equation 2) is an advection equation predicting the parallel retreat of KPs at a celerity depending on erodibility and drainage area as in Equation 10 (with $C = K$ and $p = m$, e.g. Rosenbloom and Anderson, 1994; Whipple and Tucker, 1999). With this model, a vertical step KP represents the transient response to an instantaneous baselevel fall, while a slope-break KP represents a sudden increase in baselevel fall rate (Figure 3). Because m/n ~ 0.5, p and ε should be close to 0.5. This is roughly consistent with most field data but the data for hanging valleys in the Alps ($\varepsilon = 0.8$, Valla *et al.*, 2010), the dataset on Scottish rivers by ($\varepsilon = 1.26$, Bishop *et al.*, 2005) and the Waipaoa waterfalls ($p = 1.12$, Crosby and Whipple, 2006). These examples would be more consistent with $n \sim 2$. However, when $n \neq 1$ the celerity becomes dependent on slope and the KP geometry is altered as it propagates (e.g. Finnegan, 2013; Tucker and Whipple, 2002). If $n > 1$, steeper part of the KP propagate faster and a KP will become a concave-up knickzone with a steep upstream boundary mimicking a slope-break KP. This geometry seems inconsistent with the river profiles in Scotland and in the Alps datasets, but could be consistent with the Waipaoa KPs. If $n < 1$, the opposite occurs and a KP will progressively become a convex-up knickzone migrating upstream with a sharp downstream boundary (Figure 3). Even if it seems geometrically similar to field evidence, a SPIM with $n < 1$ cannot match the transient knickzones documented in different settings as these are not migrating upstream but simply diffusing (Loget *et al.*, 2006; Ouimet *et al.*, 2007; Valla *et al.*, 2010). Therefore an empirical SPIM with $n = 1$ and $m = 0.5$ could account for the migration of KPs for many documented cases, but fail to predict the formation of knickzones for any value of m and n. Most importantly, comparison with the SS evidence highlights a fundamental inconsistency in the SPIM: SS scaling of slope with incision rate requires for most cases $n \sim 2$ and $m \sim 1$, while KP migration requires $n \sim 1$ and $m \sim 0.5$. In the subsequent section I synthesise recent theoretical developments on the theoretical derivation of the SPIM. The resulting theoretical model is then compared to the previous evidence to evaluate if the increment of model complexity improves the match with field data compared to an empirical SPIM.

Revisiting the Theoretical Derivation of the SPIM and Other Incision Models

The complexity of river incision and the upscaling issue

While the previous collection of quantitative evidence places more constraints on incision models than 15 years ago, we will likely never reach a point where an empirical model can be defined solely from the accumulated data. This underlines the need to articulate empirical evidence with the derivation of long-term incision models based on the mechanics of hydraulics, incision and sediment transport (e.g. Dietrich *et al.*, 2003; Tucker and Hancock, 2010). Yet constructing mechanistic long-term incision models has been hampered by three elements of complexity: the diversity of processes involved in river incision, the large heterogeneity of natural systems and the pronounced stochasticity of forcings (floods, sediment supply by mass wasting). Quantifying the role of these elements in long-term incision requires two forms of upscaling: a temporal upscaling of the physics derived at hydraulics timescales (e.g. flow hydraulics and incision during a flood) to geological timescales (10^4–10^6 years); and a spatial upscaling from elementary processes (e.g. rock detachment, roughness effects) to the reach scale (i.e. tens to hundreds of metres). Because the SPIM is supposed to incorporate implicitly all these complexity elements, I first start by synthesizing our understanding of the complexity of river incision in the context of the upscaling issue. Then I aim to demonstrate that the traditional approach to upscaling (which is generally no explicit upscaling at all) has resulted in incorrect formulations of the SPIM and other incision models.

Diversity of physico-chemical processes

River incision is a problem involving catchment hydrology, open flow hydraulics, sediment transport, rock mechanics (e.g. abrasion, fracturing) and rock weathering. Many of these processes are the focus of active research mobilizing their own scientific community in the larger context of earth surface processes. The reader is referred to recent reviews for entry points on these various aspects (Tucker and Hancock, 2010; Turowski, 2012; Whipple *et al.*, 2013). In terms of incision mechanisms, a variety of processes have been shown to operate in rivers and mechanistic models have been proposed for some of them: bedload and suspended load abrasion (evidence: Cook *et al.*, 2013; Hancock *et al.*, 1998; Sklar and Dietrich, 2001; models: Lamb *et al.*, 2008a; Sklar and Dietrich, 2004), fractured rock plucking (evidence: Hartshorn *et al.*, 2002; Whipple *et al.*, 2000; models: Chatanantavet and Parker, 2009; Whipple *et al.*, 2000), weathering of weak bedrock (evidence: Stock *et al.*, 2005, model: Hancock *et al.*, 2011) and incision inhibition by alluvial cover (evidence: Johnson *et al.*, 2009; Ouimet *et al.*, 2007; Turowski *et al.*, 2008b; model: Lague, 2010; Sklar and Dietrich, 2004; Turowski *et al.*, 2007). Most of these models include a dependency on shear stress either in terms of incision mechanism or because sediment transport capacity has to be evaluated. The flux of supplied sediment (which is an upstream imposed condition) is now a well-known critical element that drives and inhibits incision (tools and cover effect) which is however not explicit in the SPIM. It should also be stressed that models describing bedrock river lateral incision are lacking and that simple methods to predict shear stress patterns in complex three-dimensional geometries are only starting to emerge (Lague, 2010; Stark, 2006; Turowski *et al.*, 2009; Wobus *et al.*, 2006b). Yet, these are crucial elements to understand the dynamics of width, the emergence of hydraulic scaling and to better predict bed shear stress in mountain rivers. For instance, DiBiase and Whipple (2011) suggest that the effective value of ω_s (Equation 6), which is critical in translating discharge into bed shear stress, may actually not vary between 0 and 0.5 as in nature (see earlier): numerical simulations predicts that the varying contribution of sidewall friction for different channel geometries and flow depth translate into an effective $\omega_s \sim 0.25$, even for rectangular cross-section for which the measured $\omega_s = 0$.

Pronounced spatial heterogeneity

Steep mountain rivers are generally characterized by a large range of sediment grain sizes, a complex bed morphology, a mechanical heterogeneity of rocks over a wide range of scales (e.g. from joints to faults) and a large spatial variability in boundary conditions (uplift, sediment supply, rainfall). For reach scale incision models operating at 10 to 100 m spatial scale, the issue is to upscale the sub-reach heterogeneity to define effective parameters. These include an effective hydraulic roughness and an effective grain size that enters in the sediment transport and bedrock abrasion problems. An outstanding unresolved issue is the effective rock lithology factor that would combine the contribution of various incision processes (abrasion, plucking) modulated by rock heterogeneity characteristics (e.g. fracture density, rock mass strength variations). At present, the large heterogeneity is recognized as an important issue and has been shown to influence various aspects of incision and sediment transport processes (Goode and Wohl, 2010; Hancock *et al.*, 1998; Hodge *et al.*, 2011; Wilson *et al.*, 2013). But the upscaling itself has been hardly addressed except for the problem of hydraulic roughness (Rickenmann and Recking, 2011) and sediment transport (e.g. Nitsche *et al.*, 2011; Yager *et al.*, 2012a). In these cases the fraction of large immobile boulders to smaller frequently mobile grains is an essential effective parameter describing sub-reach heterogeneity.

Stochasticity and extreme events

River incision is driven by a wide range of discharge events imposed by meteorological forcing. The supply of sediment by hillslope mass-wasting processes in active mountain belts is also highly episodic and depends on meteorology, seismic activity and chance (e.g. Benda and Dunne, 1997; Dadson *et al.*, 2003). Quite importantly, the frequency-magnitude distribution of large discharge and mass-wasting processes tend to obey heavy-tailed distribution with a non-negligeable probability of very large extreme events (e.g. Hovius *et al.*, 1997; Turcotte and Greene, 1993) that can shift rivers in a prolonged out-of-equilibrium state either locally (e.g. landslide dam, Korup, 2006) or at catchment scale (e.g. impact of large earthquakes, Yanites *et al.*, 2010a). The trade-off between frequency and magnitude of floods and their geomorphic impact has long been recognized and an explicit upscaling proposed for alluvial rivers through the notion of effective (or dominant) discharge (Wolman and Miller, 1960). It is defined as the discharge doing most of the geomorphic work (incision or transport) and is the maximum of the product of the probability density function (PDF) of discharge and the geomorphic law considered. For bedrock rivers, it has often been postulated that extreme events are the main drivers of long-term incision resulting in a very large effective discharge (e.g. Baker and Kale, 1998). Yet, recent field data have shown that floods of annual periodicity are contributing significantly to long-term bedrock incision in Taiwan (Hartshorn *et al.*, 2002; Wilson *et al.*, 2013). Theoretical developments have also demonstrated how non-linearities can emerge over the long-term from the combination of shear-stress erosion thresholds and discharge variability requiring a careful application of the effective discharge concept (Lague *et al.*, 2005; Snyder *et al.*, 2003b;

Tucker and Bras, 2000; Tucker, 2004). These aspects are further detailed in the next section in order to best highlight their importance to the SPIM problem and beyond.

Temporal upscaling of long-term incision laws

Frequency-magnitude distribution of discharge

River discharge can vary over two- to three-orders of magnitude on a given reach owing to stochastic forcing by rainfall modulated by catchment hydrology (Figure 4). Upscaling this effect requires to have a good statistical model of these variations (a PDF). Statistics of rainfall directly reflect meteorological characteristics and have been used to predict discharge variations (e.g. Snyder *et al.*, 2003b; Tucker and Bras, 2000). However, transforming the spatio-temporal distribution of rainfall into flood hydrographs depends on a complex combination of infiltration, evapotranspiration, snowmelt processes, vegetation and catchment geomorphology. The study of discharge variability has the advantage of looking at the parameter that directly causes incision. Several authors have shown that the frequency-magnitude distribution of floods obeys a power-law relationship (Crave and Davy, 2001; Lague *et al.*, 2005; Malamud and Turcotte, 2006; Molnar *et al.*, 2006; Pandey *et al.*, 1998; Turcotte and Greene, 1993). This power-law tail does not hold at low discharges (Figure 4) and an inverse gamma PDF provides a good first-order approximation of the complete range of daily discharge (Carretier *et al.*, 2013; Crave and Davy, 2001; DiBiase and Whipple, 2011; Lague *et al.*, 2005):

$$pdf_{\overline{Q},k}(Q) = \frac{k^{k+1}}{\Gamma(k+1)} \exp\left(-k\frac{\overline{Q}}{Q}\right)\left(\frac{Q}{\overline{Q}}\right)^{-(2+k)}, \qquad (11)$$

where Γ is the gamma function, $\overline{Q}$ is the mean annual discharge and k a variability parameter (low k indicates higher discharge variability). Equation 11 predicts an asymptotic power-law distribution of floods with an exponent $-(2+k)$ which can be heavy tailed for $k < 1$ as the variance of the distribution is no more defined. A study by Molnar *et al.* (2006) have shown that in the United States, k varies between 0.01 and 5 (Figure 4) and tend to decrease with runoff (i.e. the fraction of precipitation that contributes to river discharge). Data from the western flank of the Andes fall on the same trend (Carretier *et al.*, 2013). This trend is however not valid at global scale as Taiwanese rivers exhibit high variability ($k < 1$) and large runoff (> 2 m/yr) owing to the typhoon dominated climate regime (Lague *et al.*, 2005). For $k > 2$, the inverse gamma has a light tail and is not fundamentally different from other light tails models with respect to the frequency of extreme events (e.g. exponential tail such as predicted by a Poisson rainfall model with Hortonian runoff as in Attal *et al.*, 2011; Snyder *et al.*, 2003b; Tucker and Bras, 2000 and Tucker, 2004). It is very unlikely that Equation 11 is a universal model. However, in the context of long-term incision laws, it is still quite useful, as a power-law tail yields analytical solutions of the upscaling problem which are difficult to obtain with exponential or lognormal tails.

Threshold shear stresses and the non-constant effective discharge

Apart from weathering, all fluvial geomorphic processes involved in the incision problem occur only above a critical shear stress τ_c. Of high relevance to river incision is the critical shear stress of bedload sediment transport (e.g. Buffington and Montgomery, 1997): almost all actively incising rivers have to a variable extent a cover of sediment on the river bed that must be mobilized to incise the bed. Even if the SPIM does not factor in a dependency on sediment flux (i.e. a tool or cover effect), it remains that the sediment sitting on the river bed must be mobilized for incision to occur. Hence a minimum incision threshold is the bedload entrainment threshold, although larger thresholds may exists for plucking processes (e.g. Snyder *et al.*, 2003b). This allows one to place quantitative constraints on a minimum value of τ_c based on alluvial cover grain sizes. A threshold imposes that only a fraction of the discharge events will drive incision and sediment transport (Figure 4) (Tucker and Bras, 2000). The critical discharge Q_c above which incision occurs can be estimated by (see Appendix B):

$$Q_c = \left[\left(\frac{\rho_s}{\rho_w} - 1\right)\tau_c^*\right]^{\frac{5}{3}} \cdot \frac{D_{eff}^{\frac{5}{3}}}{N} \cdot W(Q_c) \cdot S^{-\frac{7}{6}}, \qquad (12)$$

where ρ_s and D_{eff} are the density and an effective measure of grain size with respect to the mobilization of the cover, ρ_w is

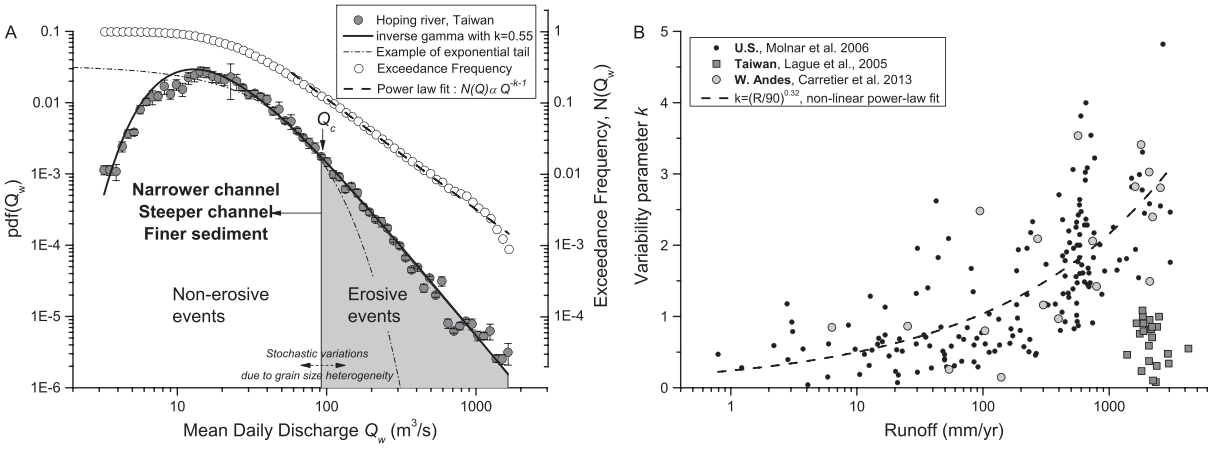

Figure 4. (A) Mean daily discharge distribution characteristics: PDF(Q_w) and exceedence frequency plot of Hoping river catchment in Taiwan (station 2560H006, 30 years record, mean annual discharge = 57 m^3/s). A critical shear stress of sediment transport imposes a minimum critical discharge Q_c for sediment transport (and incision) which is a function of channel width, slope and grain size (Equation 12). Changing one of these parameters change the range of discharge events that are causing erosion. Note that grain size heterogeneity is changing the exact value of Q_c with time. A direct fit of the PDF by an inverse gamma (Equation 11) is affected by the low discharge deviation from a pure exponential rollover (it yields $k = 0.71$). It is preferable in the context of extreme events analysis to fit a power-law to the exceedence frequency tail for which $N(Q) \sim Q^{-k-1}$ (Molnar *et al.*, 2006) which yields $k = 0.55$. (B) Daily discharge variability parameter k as a function of runoff for 155 gauging stations in the United States (Molnar *et al.*, 2006), 18 stations in the Western Andes (Carretier *et al.*, 2013) and 23 stations in Taiwan (Lague *et al.*, 2005).

the water density, N is the Manning friction coefficient and τ_c^* is the critical Shields stress. Equation 12 is fundamental to the temporal upscaling problem and illustrates the three main controls on Q_c: a slope control: Q_c is roughly inversely proportional to channel slope; a channel width control: Q_c is proportional to flow width; a grain size control: Q_c increases more than linearly with D_{eff} and decreases with the friction coefficient N.

Equation 12 neglects several aspect of sub-reach heterogeneity that are known to affect τ_c^* and the friction law used to derive it. In particular the wide range of grain sizes found in steep upland rivers yields a complex behaviour due to segregation effects (e.g. bed armouring, step pool features) that makes Q_c dependent on the history of previous discharges (e.g. Turowski *et al.*, 2011). In this context defining D_{eff} with respect to threshold problems remains an open question (e.g. Bathurst *et al.*, 1987; Ferguson, 2012). In practice, there is no consensus on choosing D_{50}, D_{84} or another measure of the grain size distribution as D_{eff} in Equation 12. It has also been shown that τ_c^* increases with slope in steep rivers (e.g. $\tau_c^*=0.15S^{0.25}$ in Lamb *et al.*, 2008) which would lower the sensitivity of Q_c on channel slope. The Manning friction law is also known to fail in steep channels at low depth to grain size ratios typical of Q_c (Ferguson, 2007; Rickenmann and Recking, 2011). For instance, average flow velocities can be overpredicted by a factor five with the Manning friction law when flow depth is of the order of D_{84} (Rickenmann and Recking, 2011). Finally, the grain shear stress can be significantly different than the cross-section averaged shear stress as the wide-channel assumption is not valid in narrow channels and large roughness elements can generate significant form drag (bedrock features, large boulders, e.g. Yager *et al.*, 2012). In addition τ_c^* will also depend on bed roughness yielding a sensitivity to the degree of alluvial cover on the bed (Ferguson, 2012; Hodge *et al.*, 2011). These additional levels of complexity related to heterogeneity may have consequences over the long-term that have not yet been evaluated.

Notwithstanding these uncertainties, Equation 12 highlights that any change through time or space of grain size, channel width or slope will change the range of discharges causing incision (Figure 4). The effect of slope has been identified as a major cause of non-linearity of long-term geomorphic laws (Lague *et al.*, 2005; Snyder *et al.*, 2003b; Tucker and Bras, 2000; Tucker, 2004): increasing slope leads to a larger range of erosive discharges, which makes their long-term integrated effect larger than if the critical discharge was constant. The same non-linearity exists for channel width but has not yet been fully recognized as all treatments of the channel width problem have neglected this aspect (see section 'Theory versus Evidence').

Comparison of analytical solutions for long-term incision laws

Let us consider an instantaneous incision law I^* (i.e. operating at hydraulic timescales) that is a function of shear stress:

$$I^* = k_e\left(\tau^a - \tau_c^a\right), \tag{13}$$

where k_e is an instantaneous erodibility factor defined at reach scale (i.e. an effective parameter). Equation 13 forms the theoretical basis of the SPIM (Howard, 1994; Whipple and Tucker, 1999) with a expected to reflect the dominant nature of incision processes (Whipple *et al.*, 2000). This theoretical prediction remains to be confronted to field/experimental data. Even if Equation 13 is an oversimplification of the actual incision processes occurring in a river, it serves to highlight how important are the effects of a shear stress threshold combined with discharge variability in the context of the SPIM and other incision models. The long-term incision rate I is given by the sum of the erosive action of all possible discharges prorated by their probability of occurrence (Tucker and Bras, 2000):

$$I = \int_{Q_c}^{Q_{max}} I^*(Q)pdf(Q)dq, \tag{14}$$

where Q_{max} is the maximum discharge possibly occurring during the timescale of integration, and Q_c is given by Equation 12. For $a \leq 3/2$, I is largely independent of Q_{max} and rapidly converges towards the long-term rate (Lague *et al.*, 2005). Two simple analytical solutions of the combination of Equations 11, 12, 13 and 14 can be obtained (Lague *et al.*, 2005): the traditional constant discharge (CD) upscaling I_c if $Q_c \sim 0$, and a threshold-stochastic (TS) upscaling I_s if Q_c is large enough for the PDF of competent discharges to be a power-law.

Constant effective discharge solution. I_c is given by (equation 19 in Lague *et al.*, 2005 with explicit channel width):

$$I_c = K_c\cdot\left(\frac{\bar{Q}}{W}\right)^{\frac{a}{\beta}n_c} S^{n_c} - k_e\tau_c^a, \text{ with} \tag{15}$$
$$K_c = k_e k_t^a \frac{\Gamma(k+1-a\alpha(1-\omega_s))}{\Gamma(k+1)k^{-a\alpha(1-\omega_s)}} \text{ and } n_c = a\beta,$$

where n_c is the slope exponent (equal to ~0.7 for a = 1 and ~1 for a = 3/2), K_c is a long-term efficiency coefficient and k_t, α, β are parameters related to the hydraulic friction law (see Appendix B). In most treatments of the problem, the critical shear stress is neglected following the assumption that the effective discharge is very large (e.g. Whipple and Tucker, 1999). In that case I_c corresponds to the traditional SPIM (CD SPIM) with an explicit description of channel width and discharge characteristics (mean and variability). The slope exponent n_c is a function of a and is expected to reflect the dominant nature of incision processes (Whipple and Tucker, 1999; Whipple *et al.*, 2000).

Threshold-stochastic solution. For large enough values of Q_c, the PDF of competent discharges can be approximated by a power-law, and an analytical solution of Equations 11, 12, 13 and 14 exists (equation 39 in Lague *et al.*, 2005 with explicit channel width inclusion):

$$I_s = K_s\cdot\left(\frac{\bar{Q}}{W}\right)^{\frac{a}{\beta}n_s} S^{n_s}, \text{ with} \tag{16}$$
$$K_s = \left(\frac{a\alpha(1-\omega_s)k_t^{\frac{n_s}{\beta}}k^{k+1}\Gamma(k+1)^{-1}}{(k+1)(k+1-a\alpha(1-\omega_s))}\right)\tau_c^{a-\frac{n_s}{\beta}}k_e,$$
$$n_s = \frac{\beta}{\alpha}\frac{k+1}{(1-\omega_s)},$$

where n_s is the slope exponent and K_s is a long-term efficiency coefficient. Equation 16 is also a SPIM with an explicit description of channel width, discharge characteristics and threshold. The complete derivation to reach a slope-area formulation of the SPIM (as in Equation 1) and relate the long-term erodibility K to the efficiency K_s is given in the section entitled 'A correctly upscaled version of the SPIM'. Because $\beta/\alpha \sim 1$ (see Appendix B) the sensitivity of I_s to width and slope is about similar. There are two fundamental differences with the constant effective discharge solution (Figure 5):

- First, there is increased non-linearity. The exponent n_s is set by the cross-sectional geometry of the river (ω_s), the discharge variability parameter k and is independent of a (Lague *et al.*, 2005). This makes n_s dependent on the type of climate and systematically larger than one: assuming an

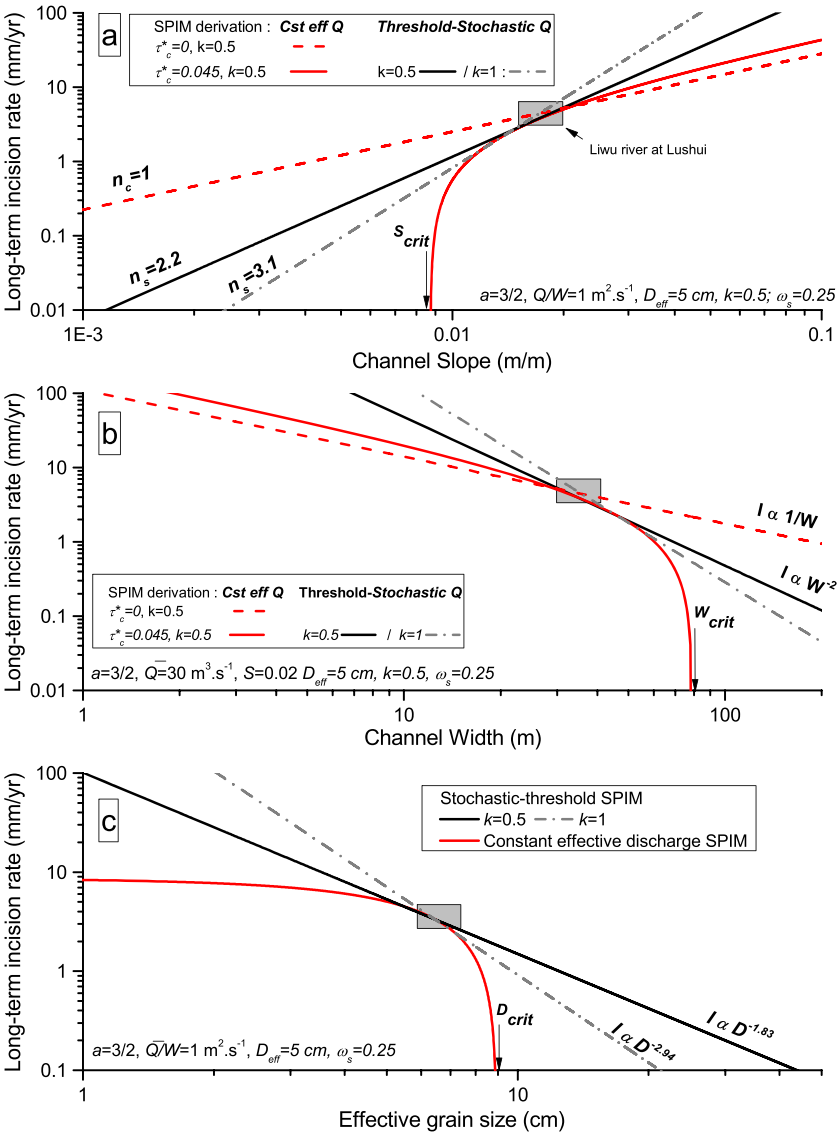

Figure 5. Comparison of threshold-stochastic and constant discharge solutions for the prediction of long-term incision rates. Each panel presents the predicted sensitivity to one parameter (slope, width and grain size) while the others are kept constant. The erodibility coefficient k_e is changed for all solutions such as predicting approximately the Liwu River conditions at LuShui ($I \sim 5$ mm/yr, $S \sim 0.02$, $D = 5$ cm, W ~ 30 m at $\bar{Q} = 30$ m^3/s, Lague, 2010). Values of k_e (in m$^{5/2}$s^2/kg$^{3/2}$) for the constant effective discharge are: $\tau^*_c = 0$, $k = 0.5$, $k_e = 1.2 \times 10^{-13}$; $\tau^*_c = 0.045$, $k = 0.5$, $k_e = 2 \times 10^{-13}$. For the threshold-stochastic solution: $\tau^*_c = 0.045$, $k = 0.5$, $k_e = 7 \times 10^{-13}$, $k = 1$, $k_e = 1.5 \times 10^{-13}$. This figure is available in colour online at wileyonlinelibrary.com/journal/espl

average value of $\omega_s = 0.25$ (Equation 6), n_s is expected to vary continuously from 1.33 to 5.33 for k ranging from 0.1 to 3 (Figure 5a). Typical values of $k = 0.5$ and $\omega_s = 0.25$ for the San Gabriel Mountains (DiBiase and Whipple, 2011) or the Liwu River (Taiwan) yield $n_s = 2.2$. The key aspect is that n_s is expected to be larger than n_c yielding more non-linear laws than the traditional CD solution with negligible threshold. This applies to the scaling of incision rate to slope (Figure 5a) but also to width (Figure 5b).

- Second, accounting for threshold effects ($\tau_c > 0$) is fundamentally different between the two solutions (Figure 5): I_s has a power-law dependency with slope, width and τ_c, while I_c has a constant threshold equal to $k_e\tau_c^a$. This generates abrupt variation of I_c in the vicinity of Q_c compared to I_s for all parameters (slope, width and grain size). Critical values of slope, width and grain size appear corresponding to $I_c = 0$ (S_{crit}, W_{crit} and D_{crit} in Figure 5). Such critical values do not emerge in I_s owing to the fact that even if the threshold becomes very large, there will always be some flood able to incise (Baldwin, 2003). Another important difference is the sensitivity of the long-term erodibility to grain size (Figure 5c): K_c is independent of τ_c, while K_s decreases strongly with grain size [as $(a - n_s/\beta) < 0$ for $a \leq 3/2$]. For the Liwu or SGM conditions and $a = 3/2$, K_s is expected to decrease roughly as $D_{eff}^{1.8}$ highlighting the important role of thresholds in governing the long-term incision efficiency.

Note that some elements of heterogeneity can be injected in Equation 16. For instance, any increase of τ^*_c with channel slope will decrease the apparent slope exponent n_s: assuming that $\tau^*_c \propto S^{0.25}$ (e.g. Lamb *et al.*, 2008), $a = 1$, $k = 0.5$, $\omega_s = 0.25$ yields an equivalent $n_s = 1.6$ rather than 2.2. Note that to get a slope exponent n_s close to one would require an extreme discharge variability ($k < 0.2$), a slope dependent critical shield stress, and $\omega_s \sim 0$. If as argued by Dibiase and Whipple (2011) the effective $\omega_s \sim 0.25$ even for rectangular cross-sections, then the smallest value of n_s would be ~ 1.25 for $k = 0$ and a slope-dependent critical shear stress.

Dominance of threshold effects in nature and consequences

Whether a constant discharge solution or threshold-stochastic solution dominates depends on how large is the normalized

critical discharge $Q_c^*=Q_c/\overline{Q}$ which can be quantified by its return time $t_r(Q_c^*)$ (DiBiase and Whipple, 2011; Lague *et al.*, 2005; Tucker, 2004). Lague *et al.* (2005) compared numerical solutions with the analytical solutions for I_c (Equation 15) and I_s (Equation 16). They found that I_c is valid if $t_r(Q_c^*) < 2$ days and that I_s is valid if $t_r(Q_c^*) > 7$ days. For $2 < t_r(Q_c^*) < 7$ days, the regime is transitional: non-linearities due to threshold-stochastic effects are significant such that the slope exponent varies progressively between n_c and n_s but there is no analytical solution for the upscaled geomorphic law (DiBiase and Whipple, 2011; Lague *et al.*, 2005). The Mendocino Triple Junction rivers, the Liwu River at Lushui and SGM rivers have been shown to have $t_r(Q_c^*) > 7$ days (DiBiase and Whipple, 2011; Lague *et al.*, 2005; Snyder *et al.*, 2003b). Later it is shown how $t_r(Q_c^*)$ can be estimated for several other published datasets considered close to SS or transient.

With an inverse gamma model such as Equation 11, $t_r(Q_c^*)$ is given by (equation 6 in Lague *et al.*, 2005a):

$$t_r\left(Q_c^*\right) = \Gamma\left(k/Q_c^*, k+1\right)^{-1}, \tag{17}$$

where $\Gamma(x,y)$ is the incomplete Gamma function. Using Equation 17, $t_r(Q_c) = 2$ days corresponds to Q_c^* ranging from 0.22 ($k = 0.1$) to 0.75 ($k = 2$) and $t_r(Q_c^*) = 7$ days corresponds to Q_c^* ranging from 0.51 ($k = 0.1$) to 1.54 ($k = 2$). Hence, as a conservative rule of thumb (if the discharge variability is not known), I_c starts to be incorrect when $Q_c^* > 0.75$, and I_s applies when $Q_c^* > 1.5$. An estimate of Q_c^* can be obtained from the reference steepness index, width index, runoff and effective grain size by combining Equations 12, 3, 7 (see Appendix B, Equation B5). From Equation B5, a steepness-width index diagram of the validity of the different upscaling solutions can be built by choosing values of Q_c^* corresponding to $t_r(Q_c^*)$=2 or 7 days and using:

$$k_{sn} = \left[\left(\frac{\rho_s}{\rho_w}-1\right)\frac{\tau_c^*}{N^\alpha}\right]^{\frac{1}{\beta}} Q_c^{*\,-\frac{\alpha(1-\omega_s)}{\beta}} \left(\frac{D_{eff}^{1/\alpha} k_{wn}}{\overline{R}}\right)^{\frac{a}{\beta}}, \tag{18}$$

with k_{wn} estimated for $b = 0.5$ and k_{sn} estimated for $\theta = 0.45$. Figure 6 shows the datasets studied earlier (Figures 1 and 2) for which there are enough constraints to estimate the various terms in Equation 18, as well as the South Fork Eel River (Sklar and Dietrich, 2006). These rivers are supposed to be close to SS but the previous analysis also applies to transient channels. KPs and knickzones of three well-documented transient rivers in the Appenine (Italy) are thus also shown (Attal *et al.*, 2011; Whittaker and Boulton, 2012; Whittaker *et al.*, 2007a). Because not all the discharge characteristics (k and $\overline{R}$), grain size or channel width measurements are available for the data in Figure 6, I have used conservative values for D_{eff} (5 cm) and the mean annual runoff (when not known) has been assumed to correspond to 75% of mean annual precipitation. This amounts at placing each data point closer to the CD domain than they likely are.

Figure 6 shows that all the SS datasets lie in the domain where threshold-stochastic effects dominate. On the opposite, KPs or knickzones of the transient Appenine rivers cover all potential domains, including the CD domain for the Celano Gorge which is the steepest and narrowest of the three rivers. The normalized steepness and width indexes of the Celano Gorge knickzone (k_{sn} ~ 320 $m^{-0.9}$, k_{wn} ~ 0.0013) are still in the domain covered by SS rivers in Figures 1 and 2. However, it is the combination of pronounced narrowing, high steepness and a small effective grain size D_{50} = 5 cm that places this reach of the river in the constant discharge upscaling regime compared to the SS rivers. Using D_{84} = 10 cm (Attal *et al.*, 2011; Whittaker *et al.*, 2007b) as the effective grain size would place the Celano Gorge in the transitional domain while the Rio Torto would be well within the threshold-stochastic

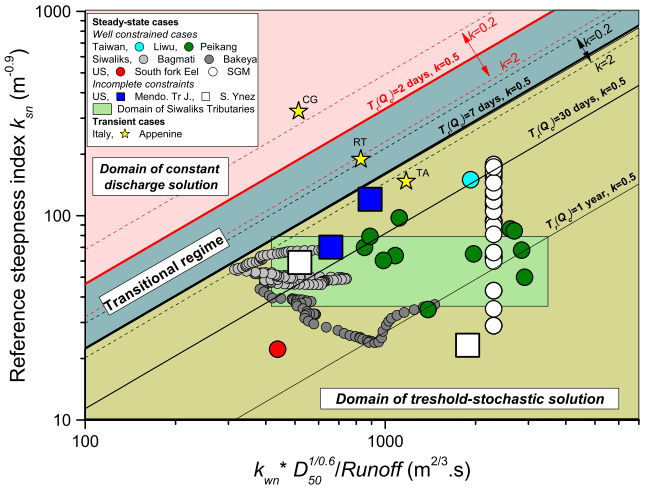

Figure 6. Steepness/modified width index diagram showing the domains of long-term upscaling solution and the position of published dataset for steady-state and transient cases (see Figure 1 for references to steady-state cases). Because some of the sites do not have a complete description of all necessary information (k, grain size D, mean annual runoff and even k_{wn} for the Siwaliks tributaries), the transition for $k = 2$ is also shown, and conservative estimates of other parameters are used when not known (D_{50} = 5 cm, runoff = 75% of mean annual precipitation, and $10^{-3} < k_{wn} < 10^{-2}$, as in Figure 2). All steady-state sites are predicted to be in the regime where a threshold-stochastic treatment of the incision problem is necessary and for which a simple analytical solution for shear-stress laws exists (Equation 16). On the opposite, knickzones and knickpoints upstream of active faults in the Appenine (Italy) cover all the possible domains, including the constant discharge domain for the steepest, narrowest river (CG: Celano Gorge, area at KP = 30 km^2, RT: Rio Torto, area at KP = 19 km^2, TA: Torrente l'Apa, area at KP = 18 km^2). Channel geometry data for the Appenine rivers from table 1 in Whittaker and Boulton (2012), D_{50} = 5 cm and precipitation rate = 0.75 m/yr as in Attal *et al.* (2011). South Fork Eel River data from Sklar and Dietrich (2004). This figure is available in colour online at wileyonlinelibrary.com/journal/espl

domain. This underlines the dominant role of grain size in governing the adequate upscaling domain compared to runoff, width and steepness. It also underlines the need to better understand the notion of effective grain size in the context of long-term channel incision.

The fact that all the SS datasets presented in Figure 6 are dominated by threshold-stochastic effects shows that the traditional CD SPIM (e.g. Howard, 1994; Whipple and Tucker, 1999) is a biased upscaling of a shear stress incision law at SS. Including a threshold in a CD solution does not solve this issue. On the contrary it generates excessive non-linearity in the vicinity of critical values of slope, width and grain size for which $I_c = 0$ (Figure 5). These critical values do not exists in a TS solution. This bias also exists for sediment flux dependent incision models as they evaluate the long-term bedload transport capacity with a shear stress law similar to Equation 13 with a = 3/2 (Chatanantavet and Parker, 2009; Sklar and Dietrich, 2004; Turowski *et al.*, 2007; Whipple and Tucker, 2002; Yanites and Tucker, 2010). In Appendix C, I present the CD and TS upscaling of long-term bedload transport capacity. I show that predictions of constant slope or width at low incision rates for SS channels are artefacts of an incorrect upscaling (Sklar and Dietrich, 2006; Turowski *et al.*, 2007, 2009; Yanites and Tucker, 2010). This statement does not question the value of the aforementioned studies in improving our description of the physics of incision and channel morphodynamics, but highlights that findings relevant to SS properties need to be re-evaluted with a proper threshold-stochastic upscaling. Note that Sklar and Dietrich (2006) use a semi-stochastic upscaling through a separation of

discharges below and above Q_c. However, by keeping Q_c constant and independent of slope or width at SS, the fundamental non-linearity emerging from the variation of Q_c with channel geometry is missing, and the solution amounts at a CD upscaling.

Neglecting threshold-stochastic effects can also bias the comparison between alongstream variations of incision rate (e.g. derived from dated terraces) and bed shear stress τ predicted for a given flood magnitude Q_R using channel slope and width (e.g. Lavé and Avouac, 2001; Yanites *et al.*, 2010b). It has been assumed that this comparison gives directly the scaling of I^* with shear stress (i.e. a). Yet, because Q_c^* is expected to vary alongstream with incision rate, the effective discharge is not constant. The threshold-stochastic solution of this problem is obtained by combining Equations 6, 16 and B1:

$$I = K_s k_t^{-\frac{n_s}{\beta}} \left(\frac{\bar{Q}}{Q_R}\right)^{k+1} \tau(Q_R)^{\frac{n_s}{\beta}}. \quad (19)$$

Equation 19 shows that if the underlying incision model is a shear stress incision law, and if all the channel reaches are in the TS domain, I is expected to increase as a power law with τ without threshold. The power-law exponent would reflect discharge variability, at-a-station hydraulic geometry and friction factors, rather than the exponent a.

Validity of the upscaled geomorphic law during transient dynamics

Because the TS solution I_s is a SPIM with explicit inclusion of discharge characteristics, channel width and grain size effects (through τ_c), it could offer a simple way to predict long-term incision rate or transport capacity without having to explicitly run a full-stochastic model. Given that the integral in Equation 14 quickly converges to the long-term value over integration time of 100 years (Lague *et al.*, 2005), it could thus be extremely useful in landscape evolution models that cannot realistically simulate channel evolution over million years with a daily timestep. Yet, the transient dynamics of threshold-stochastic models with dynamic width have hardly been explored (Attal *et al.*, 2011; Tucker, 2004; Valla *et al.*, 2010). The validity of I_s during transient dynamics is thus largely unknown.

There are at least two potential complexities emerging for the case of steep migrating KPs. First, hydraulics and incision processes may be very different in vertical step KPs: flow acceleration, plunge pool erosion, block toppling are all elements for which the physics are different than in the other less steep parts of the river (e.g. Haviv *et al.*, 2010; Lamb and Dietrich, 2009). Secondly, as observed in Figure 6 for the transient Appenine rivers, KPs and knickzones are by definition steeper but also narrower (Whittaker and Boulton, 2012; Whittaker *et al.*, 2007a). These two effects concur at reducing Q_c^* which may shift locally the river in the CD solution or transitional regime

Without the aim to fully resolve this issue, I present new stochastic simulations of the transient response to an instantaneous baselevel fall (code SSTRIM, see details in Lague, 2010; Valla *et al.*, 2010). The simulation parameters (see Figure 7) have been chosen such that at SS (U = 1 mm/yr) the normalized steepness and width indexes are within the range of data observed in Figures 1 and 2 (k_{sn} = 43.4 $m^{-0.9}$, k_{wn} = 0.022 with $k_e = 10^{-12}$ $m^{5/2}$ $s^2/kg^{3/2}$). SSTRIM computes a long-profile evolution from a series of trapezoidal cross-sections in which bank (on top of bed) incision is explicit with an additional partial differential equation for channel width. Channel width emerges dynamically and is fully dynamic as opposed to model tying uniquely width and slope (e.g. Attal *et al.*, 2008; Finnegan *et al.*, 2005) which are best described as partial dynamic width (see discussion in section entitled 'Theory versus Evidence'). Discharge varies on a daily timestep according to an inverse gamma PDF with k = 0.5 (Equation 11), and bed and bank incision are calculated according to a shear stress law such as I^* (Equation 13).

The first set of simulations (Figures 7a and 7b) presents the response to transient perturbation without threshold for which I_c applies (Equation 15). These cases are thus unrealistic as no

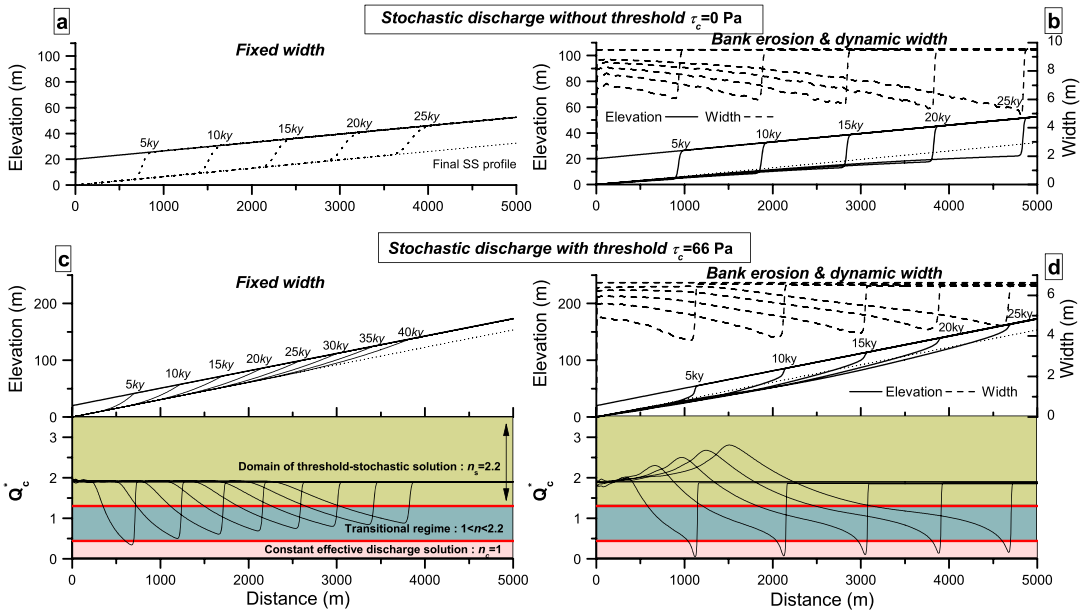

Figure 7. Illustration of the complexity of transient response to a sudden drop in baselevel of a stochastic-threshold model with fully dynamic width. Numerical solutions are obtained with the code SSTRIM (Lague, 2010; Valla *et al.*, 2010) with bed and bank incision obeying an instantaneous shear-stress incision law and no sediment flux effects. All model parameters are uniform along-stream ($\bar{R}$ = 2 m/yr, k = 0.5, $k_e = 10^{-12}$ for bed incision, $k_e = 2 \times 10^{-12}$ for bank incision, Manning coefficient N = 0.08, U = 1 mm/yr, bank angle = 75°, spatial resolution dx = 5 m). Each simulation starts from a steady-state configuration and an instantaneous baselevel fall of 20 m. (a) Standard unit stream power law model obtained by setting τ_c =0 (i.e., Q_c^* = 0), a = 1.42 and imposing a constant width. (b) Same parameters with explicit bank incision allowing width to vary dynamically. (c) and (d) Same as (a) and (b) with τ_c = 66 Pa. Lower graph represents the spatial variations of Q_c^* (Equation 12) calculated from slope and width, and showing the local upscaling regimes. This figure is available in colour online at wileyonlinelibrary.com/journal/espl

threshold is accounted for. With a constant width (Figure 7a) and a = 1.42, the model corresponds to the traditional unit SPIM with $n_c \sim 1$ given the choice of a Manning friction law (e.g. Whipple and Tucker, 1999). It shows the parallel retreat of the KP generated during the instantaneous baselevel fall with an immediate downstrem re-equilibration of the channel to SS conditions. The finite-difference method (first-order upwind scheme) and the fact that n_c is not exactly one introduces a minor numerical diffusion that alters the step geometry during propagation. Introducing dynamic width yields a narrowing of the channel in the KP with two consequences (Figure 7b): (i) the reduced width increases locally erosion efficiency which subsequently increases KP celerity (20 cm/yr compared to 15 cm/yr) (Attal *et al.*, 2008; Whittaker and Boulton, 2012) and drives the channel towards a lower slope than SS immediately downstream of the KP; (ii) the finite response time needed for the channel to widen back to its SS width introduces a delayed re-equilibration of the channel downstream of the KP. The dynamic width model also predicts the formation of a strath terrace downstream of the KP which would likely be eroded back during channel re-equilibration (assuming no lateral mobility of the channel).

The second set of experiments explores the response to the same perturbation with a realistic threshold shear stress corresponding to a grain size of 10 cm (and $\tau_c^* = 0.04$) for two cases: a constant channel width (Figure 7c) or a dynamic width (Figure 7d). The alongstream variations of Q_c^* calculated from Equation 12 are also shown in order to assess the local upscaling regime and the corresponding value for n. The initial condition is characterized by $Q_c^* = 1.9$ which places the channel within the threshold-stochastic solution domain for which $n \sim 2.2$. For the constant width run, Q_c^* is never small enough (except on the very early stages) for the CD solution to apply. It is however small enough for a large part of the knickzone to be in the transitional regime in which n increases with Q_c^* from 1 to 2.2. This result is qualitatively similar to Tucker (2004). Because $n > 1$ everywhere, the transient dynamics resembles the transient solution of SPIM models with $n > 1$ (Tucker and Whipple, 2002; Weissel and Seidl, 1997). It is not however exactly identical as n is not spatially uniform in the knickzone. The migration rate of the upstream termination of the knickzone is slower than in the case without threshold.

With dynamic width (Figure 7d), channel narrowing further decreases Q_c^* to the point where the threshold becomes negligible in the KP and a CD solution locally applies. Because $n_c = 1$ in this location, the steeper/narrower part of the KP migrates upstream in a parallel retreat mode at about the same rate as in the case without threshold (Figure 7a). With this choice of parameters the transient dynamics is thus a hybrid response of local slope-break KP migration in parallel retreat mode (n = 1) with the development of a downstream concave knickzone typical of $n > 1$. The decrease of width with incision rate in the transient zone roughly obey a power-law with an exponent varying between −0.1 to −0.25 showing that the amplitude of width reduction is not unrealistic compared to natural data (Figure 2). A downstream spatial lag in re-equilibration also exists. To my knowledge, there is no quantitative data to verify the presence and extent of this spatial lag in nature, nor was it described in previous numerical simulations that did not explicitly model bank incision.

It is beyond the scope of this paper to offer a full treatment of the transient dynamics of incision channels including different perturbations and range of parameters. My aim was to illustrate that the combination of a critical shear stress, stochastic discharge and dynamic channel width can result in a transient dynamics that cannot be captured by a single long-term upscaled model (i.e. a single set of exponents m,n). The direction of transience plays an important role: changes towards higher values of Q_c^* (e.g. decrease in uplift rate) can be modelled by a unique TS solution with $n > 1$; changes towards lower values of Q_c^* (e.g. instantaneous baselevel fall, increase in uplift rate, decrease in runoff or grain size) can possibly results in a composite transient response with locally smaller values of n in steep narrow reaches. Combined with the fact that no universal exponents are expected due to the range of k on earth, this composite response may explain why a unique incision model and set of exponents (m,n) have not been inverted from transient river profiles (e.g. Van der Beek and Bishop, 2003; Stock and Montgomery, 1999; Tomkin *et al.*, 2003). The same limitation applies to river profile inversion to infer past baselevel histories using a SPIM with n = 1 (Pritchard *et al.*, 2009; Roberts and White, 2010): n could be one in only small steep and narrow parts of the river, while being significantly larger than one elsewhere.

A correctly upscaled version of the SPIM

In this section, I derive a slope-area formulation of the threshold-stochastic SPIM to bridge the gap between Equation 1 and Equation 16. First, mean discharge and drainage area must be related through a catchment hydrology relationship:

$$\overline{Q} = R_c A^c, \tag{20}$$

where R_c and c are empirically derived constants. In small catchment with homogeneous precipitation, $c \sim 1$ and R_c is the mean annual runoff $\overline{R}$ (e.g. DiBiase and Whipple, 2011). In larger catchments or in cases with non-uniform precipitation c may differ from one (e.g. Craddock *et al.*, 2007; Roe *et al.*, 2003). Injecting Equation 20 in Equation 16, yields a slope-area formulation of a TS SPIM with explicit channel width and threshold effect (through τ_c in K_s, Equation 16):

$$I_s = K_s R_c^{\frac{a}{\beta} n_s} \cdot A^{\frac{ca}{\beta} n_s} W^{-\frac{a}{\beta} n_s} S^{n_s}. \tag{21}$$

This expression can be useful to predict SPIM incision rates from slope, drainage area, runoff, width and grain size. To obtain an expression that is solely dependent on slope as in Equation 1, one must inject an additional relationship between width and drainage area or width and slope. Because of the lack of a theoretical basis and limited field evidence for a unique width–slope relationship (see section entitled 'Theory versus Evidence'), the empirical hydraulic scaling relationship is used between width and drainage area (Equation 5) as in the original derivation of the CD SPIM (Whipple and Tucker, 1999). Because the width index k_w in Equation 5 includes a runoff effect, a discharge dependent relationship is used:

$$W = k_{wq} \overline{Q}^{b/c}, \tag{22}$$

where k_{wq} is a width factor independent of runoff which can vary with incision rate ($k_w = k_{wq} R_c^{b/c}$). Injecting Equation 22 in Equation 21 gives:

$$I_s = K A^{m_s} S^{n_s}, \text{with } K = K_s k_{wq}^{-\frac{a}{\beta} n_s} R_c^{\frac{m_s}{c}}, \tag{23}$$
$$m_s = (c - b)\frac{k+1}{1-\omega_s}, n_s = \frac{\beta}{\alpha}\frac{k+1}{1-\omega_s}$$

Equation 23 is a correctly upscaled slope-area SPIM when $Q_c^* > 1.5$, with a complete description of the erodibility coefficient K as a function of discharge characteristics (mean and variability), channel width scaling, threshold effects and instantaneous erodibility k_e. Note that the exponents m_s and n_s only depend on parameters that can be evaluated in the field: catchment hydrology, width-discharge scaling, at-a-station hydraulic geometry and discharge variability. Assuming $c \sim 1$ and $b \sim 0.3$, typical values

for m_s and n_s are 1.4 and 2.2 for high discharge variability (k = 0.5, ω_s = 0.25 as in the SGM and Liwu rivers) and 2.8 and 4.7 for very low discharge variability (k = 2, ω_s = 0.25).

An analytical solution of the erodibility coefficient such as Equation 23 can be used to unwrap the various elements composing K to estimate k_e. This requires measuring or estimating discharge characteristics ($\overline{Q}$, k), channel geometry (S, W), friction coefficient (via k_t), grain size D_{eff} and long-term incision rate I_s. At present, this calculation can only be done in a few locations where this information is available. Assuming that a = 3/2 and that $D_{eff} = D_{50}$, $k_e \sim 7\ 10^{-13}$ m$^{5/2}$ s^2/kg$^{3/2}$ in the Liwu River and $k_e \sim 2.4\ 10^{-12}$ m$^{5/2}$ s^2/kg$^{3/2}$ in the SGM (DiBiase and Whipple, 2011). It can be compared to the numerical inversion for the Rio Torto gorge (Italy) using an exponential flood distribution (Attal *et al.*, 2011) which gives $k_e \sim 2.4\ 10^{-13}$ m$^{5/2}$ s^2/kg$^{-3/2}$ for D_{eff} = 5 cm. Interestingly, the instantaneous bedrock erodibility k_e are within one-order of magnitude between these three sites and is only three times smaller in Liwu compared to the SGM despite an order of magnitude difference in incision rate and runoff (0.24 m/yr in the SGM versus 2.4 m/yr in Liwu) (Figure 1).

Reformulating Equation 23 yields a power-law relationship between slope and drainage area:

$$S = \left(\frac{I}{K_s K_{wq}^{-\frac{a}{\beta} n_s}} \right)^{\frac{1}{n_s}} R_c^{-(c-b)\frac{a}{c\beta}} A^{-(c-b)\frac{a}{\beta}}. \quad (24)$$

The previous equation can be used to compare the predictions of the TS SPIM to the SS field evidence presented earlier.

The SPIM: Theory versus Evidence

Field evidence 1: scaling of slope with drainage area

According to Equation 24, the TS SPIM predicts a concavity exponent:

$$\theta = m_s/n_s = (c-b)\frac{\alpha}{\beta}. \quad (25)$$

This theoretical prediction is identical to the traditional CD SPIM (e.g. Whipple and Tucker, 1999) and highlights that θ is mainly set by the channel width scaling with drainage area (exponent b). Given that the cause for the emergence of a width-area scaling behaviour with $b \sim$ 0.3–0.5 remains largely unknown (see later), we rely on the empirical value of b to predict θ. Even if this is not fully satisfactory, Equation 25 is an important test for the self-consistency of the TS SPIM prediction that should systematically be performed (i.e. measuring b and θ). Using the typical values of b = 0.3–0.5 yields $\theta \sim$ 0.43–0.6 for $c \sim 1$. This shows that the TS SPIM verifies this evidence and also correctly predicts that the concavity of rivers should be independent of incision rate, rock erodibility, grain size, incision law exponent a or discharge characteristics if they are uniform (and if b does not depend on them). But it also underlines that we still do not understand the physical reasons for the emergence of the observed slope and width scaling with discharge.

Field evidence 2: scaling of slope with incision rate

According to Equation 24, the TS SPIM predicts the following steepness–uplift relationship:

$$k_s = \left(\frac{I}{k_e \tau_c^{a-\frac{n_s}{b}} f(a,k)} \right)^{\frac{1}{n_s}} K_{wq}^{\frac{a}{\beta}} R_c^{-\frac{m_s}{cn_s}}, \quad (26)$$

where $f(a,k)$ is a parameter only dependent on a and k. The TS SPIM predicts a power-law relationship between channel steepness and incision rate consistent with field evidence (Equation 4) with $\varphi = 1/n_s$ (Lague *et al.*, 2005). Given that $n_s > 1$, the steepness-incision scaling exponent φ is predicted to be smaller than one which is consistent with most field evidence (Figure 1). Yet, this first order analysis neglects potential channel narrowing with incision rate (Figure 2, Duvall *et al.*, 2004). This can be accounted for by injecting the relationship between width index and incision rate (Equation 8) in Equation 26. This yields a power-law relationship between k_s and I with a reduced exponent $\varphi = 1/n_s - \alpha\chi/\beta$. To assess the consistency of this relationship with the TS SPIM, I backcalculate n_s from the observed values of φ and χ: $n_s = (\varphi + \alpha\chi/\beta)^{-1}$. In the absence of detailed information on discharge variability k in all sites but one (the SGM), the exponent n_s should be larger than one to be at least consistent with the TS SPIM prediction.

The two cases in which channel width is independent of incision rate ($\chi \sim 0$) have already been shown to be consistent with a TS SPIM: the Mendocino Triple Junction (Poisson rainfall model, Snyder *et al.*, 2003b) and the San Gabriel Mountains data (inverse gamma distribution of floods, DiBiase and Whipple, 2011). In this latter study, the predicted value of ϕ from field calibrated data (k, ω_s) matches the measured value ($\phi \sim 0.5$). However the TS SPIM fails when width decreases and slope increases with incision rate: the Santa Ynez mountains ($\chi \sim 0.68$ and $\phi \sim 0.49$, Duvall *et al.*, 2004) yield $n_s \sim 0.93$, and the Bakeya River (Lavé and Avouac, 2001) yield $n_s \sim 0.97$.

Cases in which only width varies with incision rate can also be tested ($\chi > 0$ and $\phi = 0$) although these are currently less well-constrained: in the Peikang River, $\chi \sim 0.42$ which yields $n_s \sim 2.77$, consistent with a TS SPIM. Estimates for the Bagmati are not robust enough to infer a value for n_s.

Other published datasets do not have data regarding the sensitivity of channel width with incision rate. For the datasets with $\phi < 1$, a TS SPIM could be consistent (e.g. Eastern Tibet, Ouimet *et al.*, 2009). The Siwaliks tributaries (Kirby and Whipple, 2001; Wobus *et al.*, 2006a) yield $n_s \sim 1.07$ which could be consistent with a TS SPIM with a slope dependent critical shield stress, very high discharge variability ($k \sim 0.1$) and rectangular cross-section ($\omega_s \sim 0$) (see earlier). However, any slight decrease of channel width with incision rate would yield values for $n_s < 1$ inconsistent with a TS SPIM.

Recall that in all these cases, estimates of $t_r(Q_c^*)$ are such that a TS upscaling is required (Figure 6). Hence, while it would be tempting to explain values of $n_s \leq 1$ by the traditional CD SPIM as it has been done previously (Duvall *et al.*, 2004; Kirby and Whipple, 2001; Lavé and Avouac, 2001), it is not the correct explanation (at least given our current understanding of how sediment transport thresholds operate and discharge varies in nature). Hence, the TS SPIM seems to fail as often as it works and cannot be considered a universal model. Leaving aside the Peikang River data for which the SS assumption is not well established, the TS SPIM seems to fail only when channel width significantly varies with incision rate. In those cases, other processes are involved in the definition and upscaling of the instantaneous incision law that makes n_s closer to one than expected from the TS SPIM theory.

Field evidence 3 and 4: the scaling of width with drainage area and incision rate

The previous analysis shows that the TS SPIM already fails to pass completely the second evidence level when observed channel width variations are factored in. Here I discuss briefly the current theories developed to understand the controls on channel width (and slope) and how they fare against field evidence. Two types of approaches have been pursued: inclusion of an auxiliary relationship in place of the fixed width hydraulic scaling (Finnegan *et al.*, 2005; Turowski *et al.*, 2007; Yanites and Tucker, 2010) and models of channel cross-section with an explicit calculation of bed and bank incision (e.g. Lague, 2010; Stark, 2006; Turowski *et al.*, 2009; Wobus *et al.*, 2006b). Most of these models are based on the CD SPIM, although some have introduced sediment flux effects (Turowski *et al.*, 2007; Yanites and Tucker, 2010). A first solution to the width problem was proposed by Finnegan *et al.* (2005) assuming that the width/depth ratio is constant for a given rock erodibility. This yields $W \sim Q^{3/8}S^{-3/16}$ and allows for width to decrease with incision rate (as slope increases). This auxiliary relationship was injected in the CD SPIM and results in a more non-linear relationship ($m = 0.56$, $n = 1.22$ for $a = 3/2$, rather than $m = 0.45$, $n = 1.05$, Attal *et al.*, 2008). Another approach assumes that for a given incision rate, slope is minimized with respect to width (i.e. the auxiliary relationship is $dS/dW = 0$) (Turowski *et al.*, 2007, 2009; Yanites and Tucker, 2010). This assumption corresponds to the optimization of potential energy expenditure and yields a value of $b = \theta = 0.47$, independent of the incision rate and the shear stress exponent a. It predicts that the width-depth ratio is constant and $W \sim Q^{3/8}S^{-3/16}$. Similar scaling relationships are obtained with full cross-section models using a shear-stress based incision law, although they differ in the actual SS width-depth ratio which is controlled by the partitioning of shear stress between bed and banks (Turowski *et al.*, 2009; Wobus *et al.*, 2006b). These two auxiliary relationships predict that slope increases with incision as a power-law with $\varphi \sim (1.23/a)$ and that channel width decreases with incision rate as a power-law with $\chi \sim (0.23/a)$. This cannot predict the range of values for φ and χ observed in the field (Figure 1, down to $\varphi \sim 0.5$, Figure 2, up to $\chi \sim 0.6$), nor can they predict cases in which only width (Peikang and Bagmati) or only slope varies (Mendocino and SGM) (Turowski *et al.*, 2009). They also fail in zones of transient incision where the width/depth ratio is strongly correlated to slope (Whittaker *et al.*, 2007a).

These deficiencies are expected given that these models are based on a constant discharge upscaling. Solutions involving a threshold predict constant values of width and slope at low incision rates where stochastic-threshold non-linearities would normally dominate (Turowski *et al.*, 2007, 2009; Yanites and Tucker, 2010) (Figures 6, see Appendix C). Hence, even if optimal solutions including a cover effect yield a richer behaviour than purely detachment-limited cases (Turowski *et al.*, 2007, 2009; Yanites and Tucker, 2010), their assumptions are limiting and need to be re-evaluated in a threshold-stochastic context. Yet, even if stochasticity were factored in, the optimal model solution assumes a rectangular cross-section which predicts SS geometries that are not mechanically stable: a rectangular cross-section would be stable only if bank erosion was always below a threshold. In a stochastic context this is never the case as there will always be a discharge large enough to erode banks and widen the channel. A stable SS bedrock channel geometry requires tilted banks such that the vertical component of bank erosion equates the vertical component of uplift rate (Lague, 2010; Stark, 2006; Turowski *et al.*, 2009; Wobus *et al.*, 2006b). The simplest cross-section verifying this is a trapezoidal cross-section, which can reach a unique SS geometry even with a stochastic distribution of discharge (Lague, 2010).

More importantly, an analysis of the transient dynamics predicted by SSTRIM in Figure 7d shows that even with a simple shear-stress model for bed and bank incision, there is no unique relationship between slope and width during transient dynamics (supplementary material Figure S1). By tying up slope and width with a unique static relationship, the auxiliary relationships and optimal model would not reproduce the downstream lag in re-equilibration shown in Figure 7d and may not be adapted to transient dynamics. For this reason they are best termed partial dynamic width models, as opposed to fully dynamic width model that explicitly compute bank incision.

Field evidence 5 and 6: variety of markers of transient dynamics and controls on KP migration

Owing to the reduction of the critical discharge by steepening and narrowing, KP migration can locally occur in a parallel retreat mode as in the CD SPIM model (i.e. $n = 1$), while obeying a TS SPIM elsewhere and at SS (i.e. $n > 1$, Figure 5). This composite dynamics solves an important inconsistency of the empirical SPIM discussed earlier. Note that process changes in steep KP could also introduce a composite transient dynamics of the model that have not yet been explored.

In the absence of a complete probing of the transient dynamics of the TS SPIM with bank incision, the comparison with field evidence can only be tentative. The variations of Q_c^* with slope and width offers a wide variety of recession exponents ε that could match the observed range: in very steep and narrow zone with $Q_c^* < 0.75$ the river would behave locally as a CD SPIM ($n \sim 1$) which predicts $\varepsilon \sim 0.5$. In wider and less steep KPs with $Q_c^* > 1$, the propagation would obey a non-linear SPIM with $n > 1$ which predicts values of $\varepsilon > 0.5$ and easily up to 1.5 depending on discharge variability. In this regime the celerity of KPs will also depend on slope and will increase with the intensity of the perturbation (e.g. Whipple and Tucker, 1999; Whittaker and Boulton, 2012).

Considering now the convex-up knickzones described in various settings (Figure 3, Loget *et al.*, 2006; Ouimet *et al.*, 2007; Valla *et al.*, 2010), Valla *et al.* (2010) have shown that even a TS SPIM with bank incision cannot reproduce their formation. These transient features can well be reproduced by a constant effective discharge transport-limited model (Loget *et al.*, 2006; Valla *et al.*, 2010). However a transport-limited model cannot predict the migration of vertical step and slope-break KPs and cannot be considered a more universal alternative to the SPIM. On the contrary it shows, that a universal model must accommodate both detachment-limited (advection) and transport-limited (diffusion) like behaviour to account for the diversity of transient geometries (Davy and Lague, 2009; Whipple and Tucker, 2002). A well-known element (Gilbert, 1877) to include in the incision problem on top of threshold stochastic effects and bank incision is the explicit role of sediment flux.

Beyond the SPIM: sediment flux dependent models

The previous comparison shows that the TS SPIM predictions can quantitatively match field evidence when channel width is constant. Unfortunately, this represents less than half of the existing field cases which highlights how little of the variety of geometries and dynamics met in nature can the TS SPIM match. This is not surprising given that it lacks sediment flux

effects that have been shown to play a role in inhibiting incision (e.g. Johnson *et al.*, 2009; Ouimet *et al.*, 2007; Turowski *et al.*, 2008b; Valla *et al.*, 2010) and driving incision when abrasion dominates (e.g. Cook et al., 2013; Sklar and Dietrich, 2001; Wilson *et al.*, 2013). Unfortunately, existing models including these effects (e.g. Chatanantavet and Parker, 2009; Crosby *et al.*, 2007; Gasparini *et al.*, 2006; Sklar and Dietrich, 2008, 2006; Turowski *et al.*, 2007, 2009; Whipple and Tucker, 2002; Yanites and Tucker, 2010) are based on a CD upscaling and often lack a dynamic width. These model predictions need to be fully re-evaluated in a stochastic context and with an explicit modelling of bed and bank erosion.

Such an approach has been recently conducted with the SSTRIM model to study the emergence of long-term cover effect laws from short-term variability of discharge and sediment supply (Lague, 2010). In this model k_e is modulated by the thickness of immobile sediment that is calculated by an additional dedicated mass-balance equation. The resulting long-term incision inhibition expressed as a function of $\overline{Q}_s/\overline{Q}_t$ (where $\overline{Q}_s$ is the mean bedload supply rate) is more non-linear than proposed CD solutions (Sklar and Dietrich, 2004; Turowski *et al.*, 2007): up to $\overline{Q}_s/\overline{Q}_t$ of about 0.2–0.4 the incision inhibition is limited and the SS width and slope will be equal to a TS SPIM prediction (figure 12 in Lague, 2010). This may explain the success of the TS SPIM in the SGM or in the Appenines (Attal *et al.*, 2011; DiBiase and Whipple, 2011) if we assume that abrasion is not a dominant incision process. When $\overline{Q}_s/\overline{Q}_t > 0.5$, the model predicts a rapid decrease of incision with $\overline{Q}_s/\overline{Q}_t$ and the SS slope and width will depend both on incision rate and sediment supply. These hybrid conditions (neither detachment-limited nor transport-limited) are expected in actively eroding mountain belts or river crossing active structures with large upstream draining catchment where the TS SPIM actually fails. Including a cover effect is essential to reproduce the formation of non-migrating convex knickzones as long as river incision is tightly coupled to hillslope erosion (Valla *et al.*, 2010). In that case, the model predicts another form of transient composite dynamics: owing to the strong non-linearity between $\overline{Q}_t$, slope and width (see Appendix C), $\overline{Q}_s/\overline{Q}_t$ decreases rapidly in steep narrow parts of the channel where the model shifts to detachment-limited conditions with *KP* propagation (with *ts SPIM* or *cd SPIM* mode depending on Q_c^*) (figure 13b in Valla *et al.*, 2010). Given that the cover effect has been shown to play a critical role in the partitioning between bed and bank erosion (Finnegan *et al.*, 2007; Lague, 2010; Turowski *et al.*, 2008b) the sensitivity of width and slope to incision rate is expected to be different in the hybrid regime than in the detachment limited regime and may offer a better match to field evidence.

Conclusions and Outstanding Issues

Validity and limits of the SPIM

From an empirical perspective, a single set of exponents m and n cannot account for the variety of channel response observed in nature. A non-linear SPIM with $m = 1$ and $n = 2$ could account for most observed steepness–incision relationships, but would fail to predict correctly KP propagation. Conversely a linear SPIM ($m = 0.5$, $n = 1$) would correctly predict most evidence on KP propagation, but not the SS geometry. This inconsistency can be reconciled by correctly accounting for threshold and discharge variability effects missing in the original constant discharge derivation (e.g. Howard, 1994; Whipple and Tucker, 1999). This treatment is justified by the fact that threshold-stochastic effects are predicted to always dominate at SS while some steep transient knickzones are expected to fall in the constant discharge regime (Figure 6). When channel width does not vary with incision rate, the resulting TS SPIM correctly predicts the SS scaling of slope with incision rate (DiBiase and Whipple, 2011; Snyder *et al.*, 2003b). However, when channel width decreases with incision rate, the TS SPIM apparently fails even if the actual width is used rather than a dependency with the square root of drainage area. As discussed in Whipple *et al.* (2013), examples of channel narrowing with incision rate concentrate on transient cases or river crossing zones of higher uplift rate. This highlights that the SPIM have a strict, arguably narrow, range of application (SS and uniform boundary conditions) and fails otherwise, particularly in active orogenic zones where it has been widely used (e.g. Himalayas, Taiwan).

The need for a stochastic tool and cover model

One well-known reason for the SPIM deficiency is the lack of sediment fluxes effect. We could have hoped that these effects would scale simply with drainage area and would thus be lumped in K, but the comparison with field evidence shows that it is not generally the case when boundary conditions are not uniform. Advanced mechanistic models for the tool and cover effects have been proposed, but they have not yet been fully upscaled using a stochastic description of discharge and sediment supply. Given that any sediment flux model will include a transport threshold, there is no way around a stochastic approach of this problem. A special emphasis on transient dynamics should be done as composite dynamics are expected due to the large decrease of Q_c^* and $\overline{Q}_s/\overline{Q}_t$ in steep narrow zones. Owing to the large sensitivity of TS solutions to critical shear stress, a richer spatial dynamics may also emerge from an explicit inclusion of alongstream variations of grain size (Attal and Lavé, 2009). Finally, all stochastic approaches of the incision problem have shown that the upscaled laws become significantly dependent on the variability of forcings (e.g. the slope exponent n_s) and that the detailed knowledge of functional relationships for incision transport processes may not be as important as previously expected (Lague, 2010; Lague *et al.*, 2005). This implies that depending on climate conditions, different long-term incision models (exponents, erodibility) may emerge for otherwise identical incision and transport processes. It also means that understanding the nature and cause of stochastic forcings (water and sediment) is as important as getting a correct understanding of elementary mechanisms of incision and transport.

Channel width models

Evidence shows that the range of channel width index on earth is about similar to the range of steepness index and that both parameters depend (or not) on channel incision (Figures 1 and 2). In the absence of a complete understanding of the factors controlling channel width and slope, it is thus necessary to express incision and transport laws as a function of channel slope and width (e.g. Finnegan *et al.*, 2005; Whittaker *et al.*, 2007b). *Ad hoc* width–slope relationships and optimal solution are a first improvement over simple hydraulic scaling but they do not match the variety of field constraints, lack a threshold-stochastic approach of the problem and can only be applied at SS. The problem can only be solved via the development of models with explicit bed and bank incision modulated by discharge variability and sediment flux effects. Full cross-section models offer a promising perspective for reach scale problem (e.g. Nelson and Seminara, 2011; Turowski *et al.*, 2009; Wobus et al., 2006a, 2006b). These can also begin to address the origin

and consequences of meandering in incising rivers. More computationally tractable solutions can be envisioned for landscape evolution models in which width is implicitly described at a sub-grid resolution using a trapezoidal cross-section with its own partial-differential equation (e.g. Lague, 2010; Stark, 2006). This numerical modelling effort must be complemented by the acquisition of new field data that systematically document the co-evolution of width, slope and grain size in different context, and further expand the study of incision processes with new monitoring techniques such as high accuracy LiDAR (light detection and ranging) (Lague *et al.*, 2013; Wilson *et al.*, 2013).

Heterogeneity and stochastic effects

As discussed earlier, the role of sub-reach heterogeneity in governing the reach scale incision model has hardly been addressed. To fully validate the existence of threshold-stochastic effects, it is essential to assess if the simplistic prediction of the critical discharge survives the test of natural systems (Equation 12). Quite importantly, the nearly inverse relationship between Q_c and S (Equation 12) has been documented in steep channels and flume experiments (Bathurst *et al.*, 1987) supporting a fundamental element of the TS theory. However, given our ability to detect the onset of bedload transport with impact sensors (e.g. Turowski *et al.*, 2011) or seismic noise (e.g. Burtin *et al.*, 2008), the relationship between grain size, channel width, slope and Q_c can theoretically be more extensively probed. Experiments also offer a complementary evaluation of the role of heterogeneity and the coupling between bedrock morphology, hydraulic roughness and sediment transport (e.g. Finnegan *et al.*, 2007; Johnson and Whipple, 2007), but the role of stochastic forcings has not yet been studied. Finally, terrestrial LiDAR combined with new processing techniques (e.g. Brodu and Lague, 2012), as well as sub-meter satellite imagery and airborne LiDAR altimetry open a new way to probe heterogeneity of natural systems over a wide range of scales, opening the way for a direct upscaling from centimetres to 100 m scale.

Climate control on river incision

An explicit description of discharge characteristics (mean and variability) represents a critical step towards a closer link between climate regimes and incision (Tucker and Bras, 2000). A critical element missing is a realistic description of catchment hydrology. In particular, it is time to go past the simplistic assumption that evapotranspiration is negligible (mean runoff = mean precipitation) or that it does not vary when 'climate' is changed in numerical simulations. A global analysis of precipitation (liquid and solid) and discharge datasets would provide an important empirical background to this problem. It would assess the extent to which a power-law PDF of floods systematically applies and further constrain the sensitivity of discharge variability k with climate regimes, catchment scale and catchment morphology. As discussed by Tucker and Hancock (2010), there are also potentially important couplings emerging between catchment geomorphology, channel geometry and the generation of peak discharges for otherwise identical storm events.

Final remarks

More than ever, we have reached a point where significant progress requires pluridisciplinary approaches across fields such as geomorphology, geochronology, hydrology, granular physics, rock mechanics and computer sciences. Success will likely emerge from studies managing to balance the complexity of physics, heterogeneity and stochasticity when approaching long-term dynamics. In the meantime, it is essential to use the SPIM with caution, to fully understand its limitations and to urgently work on finding its successor.

Acknowledgements—I am grateful for research support by a Marie Curie International Outgoing Fellowship within the 7th European Community Framework Programme (PIOF-GA-2009-254371). Jérôme Lavé, Brian Yanites, Eric Kirby and Mikael Attal kindly provided data and information on their study sites. Philippe Davy, Philippe Steer and Jens Turowski provided insightful comments on an earlier version of this paper. I thank Roman Dibiase, an anonymous reviewer and the Editor for comments that helped improve this paper.

Appendix A: Considerations on the Nature and Quality of the Incision Rate Data (Figure 1)

Comparing steady-state river geometry to rates of channel incision has recently benefited from the availability of catchment wide denudation rates derived from cosmogenics radionuclides (CRN) (e.g. DiBiase and Whipple, 2011; Granger *et al.*, 1996; Safran *et al.*, 2005). This adds a new tool to the traditional methods based on incision rates assumed to match independently known uplift rates (e.g. Duvall *et al.*, 2004; Kirby and Whipple, 2001; Snyder *et al.*, 2000) or measured locally from dated terraces (Lavé and Avouac, 2001; Yanites *et al.*, 2010b). They are not equal in the type of information they provide, the timescales over which they average rates and the range of incision rates they can explore. Because of the difficulty to assess steady state, incision rates derived from the assumption that they match independently known uplift rates are likely the less well constrained. Second to these are comparison with CRN denudation rates: even if a true steady-state is not attained (i.e. matching uplift rate), as long as the hillslope erosion rate matches channel incision and is relatively uniform, the comparison with channel steepness should be meaningful (e.g. DiBiase and Whipple, 2011; Ouimet *et al.*, 2009). However, CRN denudation rates are primarily measuring hillslope erosion rate over a time duration that is roughly inversely proportional to the incision rate. Hence, any mismatch between channel incision and hillslope erosion due to quaternary climate change cannot be detected. Other effects such as temporary storage of sediment, large perturbations by landslide can also affect the estimate of denudation rates (e.g. Yanites *et al.*, 2009). Hence, one of the least potentially biased source of data corresponds to locally inferred average incision rates measured over a relatively steady climate period (that is over the Holocene). This corresponds to incision rates derived from strath terraces or dated fluvially sculpted bedforms. In that case, even if the channel is not in steady-state with respect to the local baselevel lowering rate, its geometry should reflect the average incision rate locally measured since terrace abandonment. We note however that in many cases, the bedrock is rarely visible and sometime covered by up to 15 m of sediment in places in which case the channel slope may actually document the alluvial cover dynamics rather than the bedrock bed (Peikang River, Taiwan; Yanites *et al.*, 2011). Even with these uncertainties, we are now in a position to get a much more quantitative inference of the sensitivity of channel geometry to incision rates than 10 years ago.

Appendix B: Critical Discharge Calculations

Bed shear stress can be estimated in the case of steady uniform flow in a wide channel (i.e. for which the hydraulic radius is

approximately flow depth) and using an hydraulic friction law (Howard, 1994; Tucker and Bras, 2000; Willgoose *et al.*, 1991):

$$\tau = k_t \left(\frac{Q}{W(Q)}\right)^{\alpha} S^{\beta}, \tag{B1}$$

where $k_t = g\rho_w N^{3/5}$, $\alpha = 3/5$, $\beta = 7/10$ for the Manning friction law and $k_t = 8^{-1/6} g^{5/6} \rho_w f^{1/6}$, $\alpha = \beta = 2/3$ for the Darcy–Weisbach friction law, ρ_w is water density, g is gravitational acceleration, N and f are respectively the Manning and Darcy–Weisbach friction coefficients. Equation B1 may not be suitable at very high discharges for which the width/depth ratio is smaller than 20–30 and requires bank friction to be accounted for. But the critical discharge is most of the time (Figure 6) not a very large discharge, and bank friction can likely be neglected most of the time.

The critical discharge Q_c for a given width and slope is obtained by setting $\tau = \tau_c$ (Tucker, 2004). The critical shear stress τ_c is evaluated using a Shields stress criterion $\tau_c^* = 0.045$ with τ_c^* given by:

$$\tau_c^* = \frac{\tau_c}{g(\rho_s - \rho_w) D_{eff}}, \tag{B2}$$

where ρ_s and D_{eff} are the density and effective grain size of the bed cover material. Combining Equations B1 and B2 and using the Manning friction law yields:

$$Q_c = \left[\left(\frac{\rho_s}{\rho_w} - 1\right)\tau_c^*\right]^{\frac{5}{3}} \cdot \frac{D_{eff}^{\frac{5}{3}}}{N} \cdot W(Q_c) \cdot S^{-\frac{7}{6}}. \tag{B3}$$

The previous equation can be used to express the normalized critical discharge $Q_c^* = Q_c / \overline{Q}_t$ as a function of the normalized width index k_{wn} and steepness k_{sn}. Using Equations 3, 5 and 6 in Equation B3, and assuming $\overline{Q} = \overline{R}A$:

$$Q_c^* = \left[\left(\frac{\rho_s}{\rho_w} - 1\right)\frac{\tau_c^*}{N^{\alpha}} D_{eff}\right]^{\frac{1}{\alpha}} \frac{k_{wn} A^{0.5}}{\overline{R}A} \left(\frac{Q_c}{\overline{Q}}\right)^{\omega_s} \left(k_{sn} A^{-0.45}\right)^{-\frac{\beta}{\alpha}}. \tag{B4}$$

With a Manning friction law and the specific choice of reference concavity and width-drainage scaling exponents, the terms in drainage area approximately cancels out in the previous equation (they cancel out exactly for a reference concavity of 0.43). Note that with a Chezy friction law, one would need to use a reference concavity of 0.5 to get Q_c^* independent of A. Equation B4 can be reformulated as:

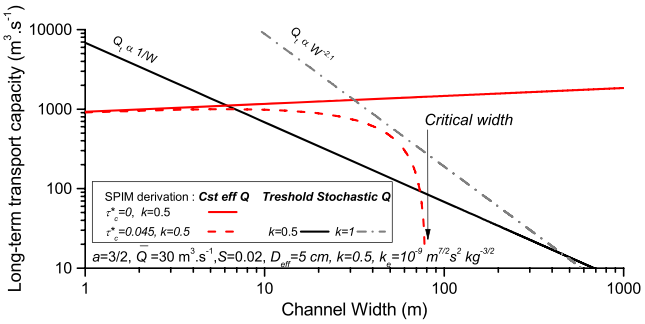

Figure 8. Sensitivity of bedload long-term transport capacity to channel width with a constant discharge and threshold stochastic upscaling. This figure is available in colour online at wileyonlinelibrary.com/journal/espl

$$Q_c^{*(1-\omega_s)} = \left(\left(\rho_s/\rho_w - 1\right)\frac{\tau_c^*}{N^{\alpha}} D_{eff}\right)^{\frac{1}{\alpha}} k_{wn} k_{sn}^{-\frac{\beta}{\alpha}} \overline{R}^{-1}, \tag{B5}$$

which can be used to estimate Q_c^* from the steepness and width indexes as well as effective grain size and mean runoff. Note that in the previous equation, Q_c^* is most sensitive to D_{eff} ($1/\alpha \sim 1.67$). Recall also that there is a potential dependency of the friction factor N on grain size.

Appendix C: Comparison of Constant Discharge and Threshold-stochastic Solutions of Long-term Bedload Transport Capacity

While predicting long-term bedload sediment transport capacity is not part of the SPIM formulation, it is a key ingredient when incorporating sediment flux effects in incision models and represents a mandatory step to go beyond the SPIM (Sklar and Dietrich, 2004; Whipple and Tucker, 2002). The instantaneous shear stress incision law (Equation 13) used to derived the SPIM has about the same formulation than many unit bedload transport capacity laws q_t when $a = 3/2$ (e.g. Meyer-Peter and Müller, 1948). We can thus reuse the constant discharge (Equation 15) and threshold-stochastic (Equation 16) prediction to estimate the long-term unit transport capacity $\overline{q}_t$. In that case k_e is a transport coefficient rather than an erodibility coefficient. The total transport capacity is obtained by multiplying $\overline{q}_t$ by channel width and yield the following solutions:

$$\overline{Q}_{ts} = K_s \cdot \overline{Q}^{\frac{a}{\beta} n_s} W^{1-\frac{a}{\beta} n_s} S^{n_s}, \text{ for the threshold-stochastic solution} \tag{C1}$$

$$\overline{Q}_{tc} = K_c \cdot \overline{Q}^{\frac{a}{\beta} n_c} W^{1-\frac{a}{\beta} n_c} S^{n_c} - W k_e \tau_c^a, \text{ for the constant discharge solution} \tag{C2}$$

where K_s and n_s are given by Equation 16, $n_c = 3\beta/2$ (~1) and K_c is given by Equation 15. Equation C1 shows that $\overline{Q}_{ts}$ is a stream power formulation. As for I_s, the slope exponent n_s depends on discharge variability and channel cross-section geometry and would typically be of the order of 1.5 to 3. This shows how the long-term transport capacity is expected to increase rapidly with minor changes in slope (Lague, 2010; Tucker, 2004). This expression differs from the traditional constant discharge upscaling resulting approximately in a linear dependency of $\overline{Q}_t$ with slope above a threshold (e.g. Sklar and Dietrich, 2004, 2006; Turowski *et al.*, 2007; Whipple and Tucker, 2002; Yanites and Tucker, 2010). Because the sensitivity with slope and critical shear stress of $\overline{Q}_{ts}$ and $\overline{Q}_{tc}$ are similar to I_s and I_c, Figures 5a and 5c directly illustrate the difference between a threshold-stochastic and constant discharge upscaling. The difference of sensitivity with width is more pronounced than between I_s and I_c owing to the multiplication by W (Figure 8): $\overline{Q}_{tc}$ increases marginally with W in the absence of threshold $\left(\overline{Q}_t \propto W^{0.1}\right)$, while $\overline{Q}_{ts} \propto W^{-1}$ for typical values of $k = 0.5$ and $\omega_s = 0.25$, or even $\overline{Q}_{ts} \propto W^{-2}$ in less variable discharge regimes ($k = 1$).

In all these cases, a threshold version of $\overline{Q}_{tc}$ predicts the existence of a critical slope, width and grain sizes corresponding to $\overline{Q}_{tc} = 0$. These critical values correspond to the constant slope (e.g. Figure 6 in Sklar and Dietrich, 2006), or constant width and slope predicted at low incision rates by constant discharge solutions of incision models using $\overline{Q}_{tc}$ ('threshold regime', Figure 4 in Turowski et al. (2007); 'Sediment-load dominated

channels', Figure 7 in Yanites and Tucker, 2010). However, owing to discharge stochasticity, there will always be a flood large enough to overcome the transport threshold and $\overline{Q}_{ts}$ predicts significant transport at low slope (resp. large width) when $\overline{Q}_{tc}$ does not (Figures 5a and 8). The threshold-stochastic upscaling does not predict the existence of critical geometries. Therefore, the prediction of asymptotic slope and width geometries at low incision rates result from an incorrect upscaling of models involving a critical shear stress.

Nomenclature

ABBREVIATIONS

SPIM	Stream Power Incision Model
SS	Steady-State
TS	Threshold-stochastic
CD	Constant discharge
KP	Knickpoint
PDF	Probability density function

EMPIRICAL SPIM

K	Long-term erodibility of the slope-area SPIM
m	Area exponent
n	Slope exponent
U	Rate of baselevel lowering
I	Long-term incision rate

CHANNEL GEOMETRY AND CHARACTERISTICS

A	Drainage area
S	Channel slope
$W(Q)$	Flow width at a given discharge Q
W	Channel width measured for a reference discharge
D_{eff}	Effective bedload grain size
k_s	Steepness index
θ	Slope-area scaling exponent (concavity index)
k_{sn}	Normalized steepness index measured with $\theta = 0.45$
φ	steepness-incision scaling exponent
k_w	Width index (defined with A)
K_{wq}	Width index (defined with $\overline{Q}$)
b	Width-area scaling exponent
k_{wn}	Normalized width index for $b = 0.5$
χ	Width-incision scaling exponent
ω_s	At-a-station width scaling exponent
ε	KP retreat-area scaling exponent
p	KP celerity scaling exponent

INSTANTANEOUS HYDRAULICS AND INCISION CHARACTERISTICS

Q	River discharge
$\overline{Q}$	Mean annual discharge
Q_R	A reference discharge
k	Discharge variability parameter
τ	Bed shear stress
τ_c	Critical shear stress
τ_c^*	Critical Shields stress
Q_c	Critical discharge at which $\tau = \tau_c$
Q_c^*	Normalized critical discharge
$t_r(Q_c^*)$	Return time of Q_c^*
N	Manning friction coefficient
α,β	Exponents of the friction law
I^*	Instantaneous incision law
a	Shear stress exponent
k_e	Instantaneous bed erodibility
k_t	Parameter combining friction, gravity and density
c	Mean discharge/drainage area scaling exponent
R_c	Proportionality coefficient between $\overline{Q}$ and A^c
$\overline{R}$	Mean annual runoff

LONG-TERM INCISION LAWS

I_c	Constant discharge prediction of I
n_c	Constant discharge prediction of n
K_c	Constant discharge incision efficiency
I_s	Threshold-stochastic prediction of I
n_s	Threshold-stochastic prediction of n
m_s	Threshold-stochastic prediction of m
K_s	Threshold-stochastic incision efficiency
$\overline{Q}_t$	Long-term bedload transport capacity
$\overline{Q}_s$	Long-term bedload sediment supply

References

Attal M, Lavé J. 2009. Pebble abrasion during fluvial transport: experimental results and implications for the evolution of the sediment load along rivers. *Journal of Geophysical Research* **114**: F04023. DOI. 10.1029/2009JF001328

Attal M, Tucker GE, Whittaker AC, Cowie PA, Roberts GP. 2008. Modeling fluvial incision and transient landscape evolution: influence of dynamic channel adjustment. *Journal of Geophysical Research* **113**: F03013. DOI. 10.1029/2007JF000893

Attal M, Cowie PA, Whittaker AC, Hobley D, Tucker GE, Roberts GP. 2011. Testing fluvial erosion models using the transient response of bedrock rivers to tectonic forcing in the Apennines, Italy. *Journal of Geophysical Research* **116**: F02005. DOI. 10.1029/2010JF001875

Baker VR, Kale VS. 1998. The role of extreme floods in shaping bedrock channels. In River Over Rocks: Fluvial Processes in Bedrock Channels, Tinkler KJ, Wohl EE (eds). AGU Monograph. American Geophysical Union: Washington, DC; 153–165.

Baldwin JA. 2003. Implications of the shear stress river incision model for the timescale of postorogenic decay of topography. *Journal of Geophysical Research* **108**: 2158. DOI. 10.1029/2001JB000550

Bathurst JC, Graf WH, Cao HH. 1987. Bedload discharge equations for steep mountain rivers. In Sediment Transport in Gravel-bed Rivers, Thorne CR, Bathurst JC, Hey RD (eds). John Wiley & Sons: Chichester; 453–491.

Benda L, Dunne T. 1997. Stochastic forcing of sediment supply to channel networks from landsliding and debris flow. *Water Resources Research* **33**: 2849–2863.

Berlin MM, Anderson RS. 2007. Modeling of knickpoint retreat on the Roan Plateau, western Colorado. *Journal of Geophysical Research* **112**: F03S06. DOI. 10.1029/2006JF000553

Bishop P, Hoey TB, Jansen JD, Artza IL. 2005. Knickpoint recession rate and catchment area: the case of uplifted rivers in Eastern Scotland. *Earth Surface Processes and Landforms* **30**: 767–778. DOI. 10.1002/esp.1191

Bookhagen B, Burbank DW. 2006. Topography, relief, and TRMM-derived rainfall variations along the Himalaya. *Geophysical Research Letters* **33**: L08405. DOI. 10.1029/2006GL026037

Bookhagen B, Strecker MR. 2012. Spatiotemporal trends in erosion rates across a pronounced rainfall gradient: examples from the

southern Central Andes. *Earth and Planetary Science Letters* **327-328**: 97–110. DOI. 10.1016/j.epsl.2012.02.005

Brocard GY, Van der Beek P. 2006. Influence of incision rate, rock strength and bedload supply on bedrock river gradients and valley-flat widths: field-based evidence and calibrations from western Alpine rivers (SE France). In Tectonics, Climate and Landscape Evolution, Willett SD, Brandon MT, Fisher D (eds). Geological Society of America Special Paper. Geological Society of America: Washington, DC; 101–126.

Brodu N, Lague D. 2012. 3D terrestrial lidar data classification of complex natural scenes using a multi-scale dimensionality criterion: Applications in geomorphology. *ISPRS Journal of Photogrammetry and Remote Sensing* **68**: 121–134. DOI. 10.1016/j.isprsjprs.2012.01.006

Buffington JM, Montgomery DR. 1997. A systematic analysis of eight decades of incipient motion studies, with special reference to gravel-bedded rivers. *Water Resources Research* **33**: 1993–2029. DOI. 10.1029/96WR03190

Burbank DW, Anderson RS. 2012. Tectonic Geomorphology, 2nd edn. Blackwell Science: Oxford.

Burtin A, Bollinger L, Vergne J, Cattin R, Nábělek JL. 2008. Spectral analysis of seismic noise induced by rivers: a new tool to monitor spatiotemporal changes in stream hydrodynamics. *Journal of Geophysical Research* **113**: B05301. DOI. 10.1029/2007JB005034

Carretier S, et al. 2013. Slope and climate variability control of erosion in the Andes of central Chile. *Geology* **41**: 195–198. DOI. 10.1130/G33735.1

Chatanantavet P, Parker G. 2009. Physically based modeling of bedrock incision by abrasion, plucking, and macroabrasion. *Journal of Geophysical Research* **114**: F04018. DOI. 10.1029/2008JF001044

Comiti F, Cadol D, Wohl E. 2009. Flow regimes, bed morphology, and flow resistance in self-formed step-pool channels. *Water Resources Research* **45**: W04424. DOI. 10.1029/2008WR007259

Cook KL, Turowski JM, Hovius N. 2013. A demonstration of the importance of bedload transport for fluvial bedrock erosion and knickpoint propagation. *Earth Surface Processes and Landforms* **38**(7): 683–695. DOI. 10.1002/esp.3313

Craddock WH, Burbank DW, Bookhagen B, Gabet EJ. 2007. Bedrock channel geometry along an orographic rainfall gradient in the upper Marsyandi River valley in central Nepal. *Journal of Geophysical Research* **112**: F03007. DOI. 10.1029/2006JF000589

Crave A, Davy P. 2001. A stochastic "precipiton" model for simulating erosion/sedimentation dynamics. *Computer and Geosciences* **27**: 815–827.

Crosby BT, Whipple KX. 2006. Knickpoint initiation and distribution within fluvial networks: 236 waterfalls in the Waipaoa River, North Island, New Zealand. *Geomorphology* **82**: 16–38. DOI. 10.1016/j.geomorph.2005.08.023

Crosby BT, Whipple KX, Gasparini NM, Wobus C. 2007. Formation of fluvial hanging valleys: Theory and simulation. *Journal of Geophysical Research* **112**: F03S10. DOI. 10.1029/2006JF000566

Cyr AJ, Granger DE. 2008. Dynamic equilibrium among erosion, river incision, and coastal uplift in the northern and central Apennines, Italy. *Geology* **36**: 103. DOI. 10.1130/G24003A.1

Cyr AJ, Granger DE, Olivetti V, Molin P. 2010. Quantifying rock uplift rates using channel steepness and cosmogenic nuclide-determined erosion rates: examples from northern and southern Italy. *Lithosphere* **2**: 188–198. DOI. 10.1130/L96.1

Dadson S, et al. 2003. Links between erosion, runoff variability and seismiciy in the Taiwan orogen. *Nature* **426**: 648–651. DOI. 10.1038/nature02150

Davy P, Lague D. 2009. Fluvial erosion/transport equation of landscape evolution models revisited. *Journal of Geophysical Research* **114**: F03007. DOI. 10.1029/2008JF001146

DiBiase RA, Whipple KX. 2011. The influence of erosion thresholds and runoff variability on the relationships among topography, climate, and erosion rate. *Journal of Geophysical Research* **116**: F04036. DOI. 10.1029/2011JF002095

DiBiase RA, Whipple KX, Heimsath AM, Ouimet WB. 2010. Landscape form and millennial erosion rates in the San Gabriel Mountains, CA. *Earth and Planetary Science Letters* **289**: 134–144. DOI. 10.1016/j.epsl.2009.10.036

Dietrich WE, Bellugi D, Sklar LS, Stock J, Heimsath A, Roering JJ. 2003. Geomorphic transport laws for predicting landscape form and dynamics. In Prediction in Geomorphology, Wilcock RP (ed). American Geophysical Union: Washington, DC.

Duvall A, Kirby E, Burbank DW. 2004. Tectonic and lithologic controls on bedrock channel profiles and processes in coastal California. *Journal of Geophysical Research* **109**: F03002. DOI. 10.1029/2003JF000086

Ferguson R 2007. Flow resistance equations for gravel- and boulder-bed streams. *Water Resources Research* **43**: W05427. DOI. 10.1029/2006wr005422

Ferguson RI. 2012. River channel slope, flow resistance, and gravel entrainment thresholds. *Water Resources Research* **48**: W05517. DOI. 10.1029/2011WR010850

Finnegan NJ. 2013. Interpretation and downstream correlation of bedrock river terrace treads created from propagating knickpoints. *Journal of Geophysical Research* **118**: 54–64. DOI. 10.1029/2012JF002534

Finnegan NJ, Roe GH, Montgomery DR, Hallet B. 2005. Controls on the channel width of rivers: implications for modeling fluvial incision of bedrock. *Geology* **33**: 229–232.

Finnegan NJ, Sklar LS, Fuller TK. 2007. Interplay of sediment supply, river incision, and channel morphology revealed by the transient evolution of an experimental bedrock channel. *Journal of Geophysical Research* **112**: F03S11. DOI. 10.1029/2006JF000569

Flint J-J 1974. Stream gradient as a function of order, magnitude, and discharge. *Water Resources Research* **10**: 969–973.

Garcia-Castellanos D, Villaseñor a. 2011. Messinian salinity crisis regulated by competing tectonics and erosion at the Gibraltar arc. *Nature* **480**: 359–63.

Gardner TW. 1983. Experimental study of knickpoint and longitudinal profile evolution in cohesive, homogeneous material. *Geological Society of America Bulletin* **94**: 664–672.

Gasparini NM, Bras RL, Whipple KX. 2006. Numerical modeling of non-steady-state river profile evolution using a sediment-flux-dependent incision model. In Tectonics, Climate and Landscape Evolution, Willett SD, Brandon MT, Fisher D (eds). Geological Society of America Special Papers. Geological Society of America: Washington, DC; 127–141.

Gilbert G. 1877. Report on the Geology of the Henry Mountains. US Government Printing Office: Washington, DC.

Goode JR, Wohl E. 2010. Coarse sediment transport in a bedrock channel with complex bed topography. *Water Resources Research* **46**: 1–14. DOI. 10.1029/2009WR008135

Granger DE, Kirchner JW, Finkel R. 1996. Spatially averaged long-term erosion rates measured from in situ-produced cosmogenic nuclides in alluvial sediment. *The Journal of Geology* **104**: 249–257. DOI. 10.1086/629823

Hancock GS, Anderson RS. 2002. Numerical modeling of fluvial strath-terrace formation in response to oscillating climate. *Geological Society of America Bulletin* **114**: 1131–1142. DOI. 10.1130/0016-7606(2002)

Hancock GS, Anderson RS, Whipple KX. 1998. Beyond power: bedrock river incision process and form. In River Over Rocks, Tinkler KJ, Wohl EE (eds), AGU Monograph. American Geophysical Union: Washington, DC; 35–60.

Hancock GS, Small EE, Wobus C. 2011. Modeling the effects of weathering on bedrock-floored channel geometry. *Journal of Geophysical Research* **116**: F03018. DOI. 10.1029/2010JF001908

Harkins N, Kirby E, Heimsath A, Robinson R, Reiser U. 2007. Transient fluvial incision in the headwaters of the Yellow River, northeastern Tibet, China. *Journal of Geophysical Research* **112**: F03S04. DOI. 10.1029/2006JF000570

Hartshorn K, Hovius N, Dade WB, Slingerland RL. 2002. Climate-driven bedrock incision in an active mountain belt. *Science* **297**: 2036–8.

Haviv I, Enzel Y, Whipple KX, Zilberman E, Matmon A, Stone J, Fifield KL. 2010. Evolution of vertical knickpoints (waterfalls) with resistant caprock: insights from numerical modeling. *Journal of Geophysical Research* **115**: F03028. DOI. 10.1029/2008JF001187

Hayakawa Y, Matsukura Y. 2003. Recession rates of waterfalls in Boso Peninsula, Japan, and a predictive equation. *Earth Surface Processes and Landforms* **28**: 675–684. DOI. 10.1002/esp.519

Herman F, Braun J. 2006. Fluvial response to horizontal shortening and glaciations: a study in the Southern Alps of New Zealand. *JGR-Earth Surface* **111**: F01008. DOI. 10.1029/2004JF000248

Hodge RA, Hoey TB, Sklar LS. 2011. Bed load transport in bedrock rivers: the role of sediment cover in grain entrainment, translation, and deposition. *Journal of Geophysical Research* **116**: F04028. DOI. 10.1029/2011JF002032

Hovius N, Stark CP, Allen PA. 1997. Sediment flux from a mountain belt derived by landslide mapping. *Geology* **25**: 231–234.

Howard AD. 1994. A detachment-limited model of drainage basin evolution. *Water Resources Research* **30**: 2261–2285.

Howard AD, Kerby G. 1983. Channel changes in badlands. *Geological Society of America Bulletin* **94**: 739–752.

Jansen JD, Fabel D, Bishop P, Xu S, Schnabel C, Codilean AT. 2011. Does decreasing paraglacial sediment supply slow knickpoint retreat? *Geology* **39**: 543–546. DOI. 10.1130/G32018.1

Johnson JP, Whipple KX. 2007. Feedbacks between erosion and sediment transport in experimental bedrock channels. *Earth Surface Processes and Landforms* **32**: 1048–1062. DOI. 10.1002/esp.1471

Johnson JPL, Whipple KX, Sklar LS, Hanks TC. 2009. Transport slopes, sediment cover, and bedrock channel incision in the Henry Mountains, Utah. *Journal of Geophysical Research* **114**: F02014. DOI. 10.1029/2007jf000862

Kirby E, Whipple K. 2001. Quantifying differential rock-uplift rates via stream profile analysis. *Geology* **29**: 415–418.

Kirby E, Whipple KX. 2012. Expression of active tectonics in erosional landscapes. *Journal of Structural Geology* **44**: 54–75. DOI. 10.1016/j.jsg.2012.07.009

Knighton D. 1998. Fluvial Form and Processes. Arnold, Hodder Headline: London.

Korup O 2006. Rock-slope failure and the river long profile. *Geology* **34**: 45–48. DOI. 10.1130/g21959.1

Lague D 2010. Reduction of long-term bedrock incision efficiency by short-term alluvial cover intermittency. *Journal of Geophysical Research* **115**: F02011. DOI. 10.1029/2008JF001210

Lague D, Davy P. 2003. Constraints on the long-term colluvial erosion law by analyzing slope–area relationships at various tectonic uplift rates in the Siwaliks Hills (Nepal). *Journal of Geophysical Research* **108**(B2): 2129. DOI. 10.1029/2002JB001893

Lague D, Davy P, Crave A. 2000. Estimating uplift rate and erodibility from the area–slope relationship: examples from Brittany (France) and numerical modelling. *Physics and Chemistry of the Earth (A)* **25**: 543–548.

Lague D, Crave A, Davy P. 2003. Laboratory experiments simulating the geomorphic response to tectonic uplift. *Journal of Geophysical Research* **108**. DOI.10.1029/2002JB001785

Lague D, Hovius N, Davy P. 2005. Discharge, discharge variability, and the bedrock channel profile. *Journal of Geophysical Research* **110**: F04006. DOI. 10.1029/2004JF000259

Lague D, Brodu N, Leroux J. 2013. Accurate 3D comparison of complex topography with terrestrial laser scanner: application to the Rangitikei canyon (N-Z). *ISPRS Journal of Photogrammetry and Remote Sensing* **82**: 10–26. DOI. 10.1016/j.isprsjprs.2013.04.009

Lamb MP, Dietrich WE. 2009. The persistence of waterfalls in fractured rock. *Geological Society of America Bulletin* **121**: 1123–1134. DOI. 10.1130/B26482.1

Lamb MP, Dietrich WE, Sklar LS. 2008a. A model for fluvial bedrock incision by impacting suspended and bed load sediment. *Journal of Geophysical Research* **113**: F03025. DOI. 10.1029/2007JF000915

Lamb MP, Dietrich WE, Venditti JG. 2008b. Is the critical Shields stress for incipient sediment motion dependent on channel-bed slope? *Journal of Geophysical Research* **113**: F02008. *DOI.* 10.1029/2007JF000831

Lavé J, Avouac JP. 2001. Fluvial incision and tectonic uplift across the Himalayas of central Nepal. *Journal of Geophysical Research* **106**: 26,526–26,591. DOI. 10.1029/2001JB000359

Leopold LB, Maddock TJ. 1953. The hydraulic geometry of stream channels and some physiographic implications. U.S. Geological Survey Professional Paper 52.

Loget N, Van den Driessche J. 2009. Wave train model for knickpoint migration. *Geomorphology* **106**: 376–382. DOI. 10.1016/j.geomorph.2008.10.017

Loget N, Davy P, Van den Driessche J. 2006. Mesoscale fluvial erosion parameters deduced from modeling the Mediterranean sea level drop during the Messinian (late Miocene). *Journal of Geophysical Research* **111**: F03005. DOI. 10.1029/2005JF000387

Malamud B, Turcotte D. 2006. The applicability of power-law frequency statistics to floods. *Journal of Hydrology* **322**: 168–180. DOI. 10.1016/j.jhydrol.2005.02.032

Meyer-Peter E, Müller R. 1948. Formulas for bedload transport. *Proceedings of the 2nd. Meeting of the International Association of Hydraulic Research, Stockholm* **3**: 39–64.

Miller SR, Baldwin SL, Fitzgerald PG. 2012. Transient fluvial incision and active surface uplift in the Woodlark Rift of eastern Papua New Guinea. *Lithosphere* **4**: 131–149. DOI. 10.1130/L135.1

Molnar P, Anderson RS, Kier G, Rose J. 2006. Relationships among probability distributions of stream discharges in floods, climate, bed load transport, and river incision. *Journal of Geophysical Research* **111**: F02001. DOI. 10.1029/2005JF000310

Montgomery DR, Foufoula-Georgiou E. 1993. Channel network source representation using digital elevation models. *Water Resources Research* **29**: 3925–3934.

Montgomery DR, Gran KB. 2001. Downstream variations in the width of bedrock channels. *Water Resources Research* **37**: 1841–1846.

Nelson PA, Seminara G. 2011. Modeling the evolution of bedrock channel shape with erosion from saltating bed load. *Geophysical Research Letters* **38**: L17406. DOI. 10.1029/2011GL048628

Niemi NA, Oskin M, Burbank DW, Heimsath AM, Gabet EJ. 2005. Effects of bedrock landslides on cosmogenically determined erosion rates. *Earth and Planetary Science Letters* **237**: 480–498. DOI. 10.1016/j.epsl.2005.07.009

Nitsche M, Rickenmann D, Turowski JM, Badoux A, Kirchner JW. 2011. Evaluation of bedload transport predictions using flow resistance equations to account for macro-roughness in steep mountain streams. *Water Resources Research* **47**: W08513. DOI. 10.1029/2011WR010645

Ouimet WB, Whipple KX, Royden LH, Sun Z, Chen Z. 2007. The influence of large landslides on river incision in a transient landscape: eastern margin of the Tibetan Plateau (Sichuan, China). *Geological Society of America Bulletin* **119**: 1462–1476. DOI. 10.1130/B26136.1

Ouimet WB, Whipple KX, Granger DE. 2009. Beyond threshold hillslopes: channel adjustment to base-level fall in tectonically active mountain ranges. *Geology* **37**: 579–582. DOI. 10.1130/G30013A.1

Pandey G, Loveyjoy S, Schertzer D. 1998. Multifractal analysis of daily river flows including extremes for basins of five to two million square kilometres, one day to 75 years. *Journal of Hydrology* **208**: 62–81.

Perron JT, Royden L. 2013. An integral approach to bedrock river profile analysis. *Earth Surface Processes and Landforms* **38**: 570–576. DOI. 10.1002/esp.3302

Pritchard D, Roberts GG, White NJ, Richardson CN. 2009. Uplift histories from river profiles. *Geophysical Research Letters* **36**: 1–5. DOI. 10.1029/2009GL040928

Ramsey LA, Hovius N, Lague D, Liu C-S. 2006. Topographic characteristics of the submarine Taiwan orogen. *Journal of Geophysical Research* **111**: F02009. DOI. 10.1029/2005JF000314

Rickenmann D, Recking A. 2011. Evaluation of flow resistance in gravel-bed rivers through a large field data set. *Water Resources Research* **47**: W07538. DOI. 10.1029/2010wr009793

Roberts GG, White N. 2010. Estimating uplift rate histories from river profiles using African examples. *Journal of Geophysical Research* **115**: B02406. DOI. 10.1029/2009JB006692

Roe GH, Montgomery DR, Hallet B. 2003. Orographic precipitation and the relief of mountain ranges. *Journal of Geophysical Research* **108**: 2315. DOI. 10.1029/2001JB001521

Rosenbloom NA, Anderson RS. 1994. Hillslope and channel evolution in a marine terraced landscape, Santa Cruz, California. *Journal of Geophysical Research* **99**: 14013–14029.

Safran EB, Bierman PR, Aalto R, Dunne T, Whipple KX, Caffee M. 2005. Erosion rates driven by channel network incision in the Bolivian Andes. *Earth Surface Processes and Landforms* **30**: 1007–1024. DOI. 10.1002/esp.1259

Seidl MA, Dietrich WE, Kirchner JW. 1994. Longitudinal profil development into bedrock: an analysis of Hawaiian Channels. *The Journal of Geology* **102**: 457–474.

Sklar LS, Dietrich WE. 2001. Sediment and rock strength controls on river incision into bedrock. *Geology* **29**: 1087–1090.

Sklar LS, Dietrich WE. 2004. A mechanistic model for river incision into bedrock by saltating bed load. *Water Resources Research* **40**: W06301. DOI. 10.1029/2003WR002496

Sklar LS, Dietrich WE. 2006. The role of sediment in controlling steady-state bedrock channel slope: implications of the saltation-abrasion incision model. *Geomorphology* **82**: 58–83. DOI. 10.1016/j.geomorph.2005.08.019

Sklar L, Dietrich W. 2008. Implications of the saltation–abrasion bedrock incision model for steady-state river longitudinal profile

relief and concavity. *Earth Surface Processes and Landforms* **33**: 1129–1151. DOI. 10.1002/esp.1689

Snyder NP, Whipple KX, Tucker GE, Merritts DJ. 2000. Landscape response to tectonic forcing: DEM analysis of stream profiles in the Mendocino triple junction region, northern California. *Geological Society of America Bulletin* **112**: 1250–1263.

Snyder NP, Whipple KX, Tucker GE, Merritts DJ. 2003a. Channel response to tectonic forcing: field analysis of stream morphology and hydrology in the Mendocino triple junction region, northern California. *Geomorphology* **53**: 97–127. DOI. 10.106/S0169-555X(02)00349-5

Snyder NP, Whipple KX, Tucker GE, Merritts DJ. 2003b. Importance of a stochastic distribution of floods and erosion thresholds in the bedrock river incision problem. *Journal of Geophysical Research* **108**: 2117. DOI. 10.1029/2001JB001655

Stark CP. 2006. A self-regulating model of bedrock river channel geometry. *Geophysical Research Letters* **33**: L04402. DOI. 10.1029/2005GL023193

Sternai P, Herman F, Champagnac J. 2012. Pre-glacial topography of the European Alps. *Geology* **40**: 1067–1070. DOI. 10.1130/G33540.1

Stock J, Dietrich WE. 2003. Valley incision by debris flows: evidence of a topographic signature. *Water Resources Research* **39**: 1089. DOI. 10.1029/2001WR001057

Stock JD, Montgomery DR. 1999. Geologic constraints on bedrock river incision using the stream power law. *Journal of Geophysical Research* **104**: 4983–4993.

Stock JD, Montgomery DR, Collins BD, Dietrich WE, Sklar L. 2005. Field measurements of incision rates following bedrock exposure: implications for process controls on the long profiles of valleys cut by rivers and debris flows. *Geological Society of America Bulletin* **117**: 174. DOI. 10.1130/B25560.1

Tomkin JH, Brandon MT, Pazzaglia FJ, Barbour JR, Willett SD. 2003. Quantitative testing of bedrock incision models for the Clearwater River, NW Washington State. *Journal of Geophysical Research* **108**: 2308.

Tucker GE. 2004. Drainage basin sensitivity to tectonic and climatic forcing: implications of a stochastic model for the role of entrainment and erosion thresholds. *Earth Surface Processes and Landforms* **29**: 185–205. DOI. 10.1002/esp.1020

Tucker GE, Bras RL. 2000. A stochastic approach to modeling the role of rainfall variability in drainage basin evolution. *Water Resources Research* **36**: 1953–1964.

Tucker GE, Hancock GR. 2010. Modelling landscape evolution. *Earth Surface Processes and Landforms* **35**: 28–50. DOI. 10.1002/esp.1952

Tucker GE, Whipple KX. 2002. Topographic outcomes predicted by stream erosion models: sensitivity analysis and intermodel comparison. *Journal of Geophysical Research* **107**: 2179. DOI. 10.1029/2001JB000162

Turcotte DL, Greene L. 1993. A scale-invariant approach to flood-frequency analysis. *Stochastic Hydrology and Hydraulics* **7**: 33–40.

Turowski JM. 2012. Semi-alluvial channels and sediment-flux-driven bedrock erosion. In Gravel-bed Rivers: Processes, Tools, Environments, Church M, Biron PM, Roy AG (eds). John Wiley & Sons: Chichester; 401–416.

Turowski J, Lague D, Crave A, Hovius N. 2006. Experimental channel response to tectonic uplift. *Journal of Geophysical Research* **111**: F03008. DOI. 10.1029/2005JF000306

Turowski JM, Lague D, Hovius N. 2007. Cover effect in bedrock abrasion: a new derivation and its implications for the modeling of bedrock channel morphology. *Journal of Geophysical Research* **112**: F04006. DOI. 10.1029/2006JF000697

Turowski J, Hovius N, Wilson A, Horng MJ. 2008a. Hydraulic geometry, river sediment and the definition of bedrock channels. *Geomorphology* **99**: 26–38. DOI. 10.106/j.geomorph.2007.10.001

Turowski JM, Hovius N, Hsieh M-L, Lague D, Chen M-C. 2008b. Distribution of erosion across bedrock channels. *Earth Surface Processes and Landforms* **33**: 353–363. DOI. 10.1002/esp.1559

Turowski JM, Lague D, Hovius N. 2009. Response of bedrock channel width to tectonic forcing: insights from a numerical model, theoretical considerations, and comparison with field data. *Journal of Geophysical Research* **114**: F03016. DOI. 10.1029/2008JF001133

Turowski JM, Badoux A, Rickenmann D. 2011. Start and end of bedload transport in gravel-bed streams. *Geophysical Research Letters* **38**: L04401. DOI. 10.1029/2010GL046558

Valla P, Van der Beek P, Lague D. 2010. Fluvial incision into bedrock: insights from morphometric analysis and numerical modeling of gorges incising glacial hanging valleys (Western Alps, France). *Journal of Geophysical Research* **115**: F02010. DOI. 10.1029/2008JF001079

Van der Beek P, Bishop P. 2003. Cenozoic river profile development in the Upper Lachlan catchment (SE Australia) as a test of quantitative fluvial incision models. *Journal of Geophysical Research* **108**: 2309. DOI. 10.1029/2002JB002125

Weissel JK, Seidl MA. 1997. Influence of rock strength properties on escarpment retreat across passive continental margins. *Geology* **25**: 631–634.

Whipple KX. 2004. Bedrock rivers and the geomorphology of active orogens. *Annual Review of Earth and Planetary Sciences* **32**: 151–185. DOI. 10.1146/annurev.earth.32.101802.120356

Whipple K, Meade B. 2006. Orogen response to changes in climatic and tectonic forcing. *Earth and Planetary Science Letters* **243**: 218–228. DOI. 10.1016/j.epsl.2005.12.022

Whipple KX, Tucker GE. 1999. Dynamics of the stream-power river incision model: implications for height limits of mountain ranges, landscape response timescales, and research needs. *Journal of Geophysical Research* **104**: 17,617–17,674.

Whipple KX, Tucker GE. 2002. Implications of sediment-flux-dependent river incision models for landscape evolution. *Journal of Geophysical Research* **107**. DOI. 10.1029/2000JB000044

Whipple KX, Hancock GS, Anderson RS. 2000. River incision into bedrock: mechanics and relative efficacy of plucking, abrasion, and cavitation. *Geological Society of America Bulletin* **112**: 490–503. DOI. 10.1130/0016-7606(2000)112<490:RIIBMA>2.0.CO;2

Whipple KX, Dibiase RA, Crosby BT. 2013. Bedrock rivers. In Treatise on Geomorphology, Schroder J, Wohl E (eds). Academic Press: San Diego, CA; 550–573.

Whittaker AC, Boulton SJ. 2012. Tectonic and climatic controls on knickpoint retreat rates and landscape response times. *Journal of Geophysical Research* **117**: F02024. DOI. 10.1029/2011JF002157

Whittaker AC, Cowie PA, Attal M, Tucker GE, Roberts GP. 2007a. Bedrock channel adjustment to tectonic forcing: implications for predicting river incision rates. *Geology* **35**: 103–106. DOI. 10.1130/G20738.1

Whittaker AC, Cowie PA, Attal M, Tucker GE, Roberts GP. 2007b. Contrasting transient and steady-state rivers crossing active normal faults: new field observations from the Central Apennines, Italy. *Basin Research* **19**: 529–556. DOI. 10.1111/j.1365-2117.2007.00337.x

Willgoose G, Bras RL, Rodríguez-Iturbe I. 1991. A coupled channel network growth and hillslope evolution model: 1. Theory. *Water Resources Research* **27**: 1671–1684.

Wilson A, Hovius N, Turowski JM. 2013. Upstream-facing convex surfaces: bedrock bedforms produced by fluvial bedload abrasion. *Geomorphology* **180-181**: 187–204. DOI. 10.1016/j.geomorph.2012.10.010

Wobus C, Hodges KV, Whipple KX. 2003. Has focused denudation sustained active thrusting at the Himalayan topographic front? *Geology* **31**: 861–864.

Wobus C, Whipple KX, Kirby E, Snyder N, Johnson J, Spyropolou K, Crosby B, Sheehan D. 2006a. Tectonics from topography: procedures, promise, and pitfalls. In Tectonics, Climate, and Landscape Evolution, Willett SD, Hovius N, Brandon MT, Fisher D (eds). Geological Society of America Special Paper 398. Geological Society of America: Washington, DC; 55–74.

Wobus CW, Tucker GE, Anderson RS. 2006b. Self-formed bedrock channels. *Geophysical Research Letters* **33**: 0–5. DOI. 10.1029/2006GL027182

Wohl E, David GCL. 2008. Consistency of scaling relations among bedrock and alluvial channels. *Journal of Geophysical Research* **113**: F04013. DOI. 10.1029/2008JF000989

Wolman MG, Miller JP. 1960. Magnitude and frequency of forces in geomorphic processes. *Journal of Geology* **68**: 54–74.

Yager EM, Dietrich WE, Kirchner JW, McArdell BW. 2012. Prediction of sediment transport in step-pool channels. *Water Resources Research* **48**: W01541. DOI. 10.1029/2011WR010829

Yanites BJ, Tucker GE. 2010. Controls and limits on bedrock channel geometry. *Journal of Geophysical Research* **115**: F04019. DOI. 10.1029/2009jf001601

Yanites BJ, Tucker GE, Anderson RS. 2009. Numerical and analytical models of cosmogenic radionuclide dynamics in landslide-dominated drainage basins. *Journal of Geophysical Research* **114**: F01007. DOI. 10.1029/2008JF001088

Yanites BJ, Tucker GE, Mueller KJ, Chen Y. 2010a. How rivers react to large earthquakes: evidence from central Taiwan. *Geology* **38**(7): 639–642. DOI. 10.1130/G30883.1

Yanites BJ, Tucker GE, Mueller KJ, Chen YG, Wilcox T, Huang SY, Shi KW. 2010b. Incision and channel morphology across active structures along the Peikang River, central Taiwan: implications for the importance of channel width. *Geological Society of America Bulletin* **122**: 1192–1208. DOI. 10.1130/B30035.1

Yanites BJ, Tucker GE, Hsu H-L, Chen C, Chen Y-G, Mueller KJ. 2011. The influence of sediment cover variability on long-term river incision rates: an example from the Peikang River, central Taiwan. *Journal of Geophysical Research* **116**: 1–13. DOI. 10.1029/2010JF001933

Supporting Information

Additional supporting information may be found in the online version of this article at the publisher's web site.